JGR Solid Earth

RESEARCH ARTICLE
10.1029/2025JB032561

Key Points:

- Hilina Pali is documented in unprecedented high resolution in lake sediments from the polar Urals
- In northern Russia virtual geomagnetic pole (VGP) latitudes remained higher than 55°N during Hilina Pali
- Hilina Pali (defined by VGP latitude) took place 20.3 to 19.0 ka cal. BP and lasted 1294 ± 44 years according to varve counting

Correspondence to:
S. Scheidt,
stephanie.scheidt@uni-koeln.de

Citation:
Scheidt, S., Ólafsdóttir, S., Brendryen, J., Nowaczyk, N. R., Lenz, M. M., Svendsen, J. I., & Haflidason, H. (2025). New insights into the proposed geomagnetic excursion Hilina Pali from high-resolution lake sediment cores from the polar Ural Mountains, Arctic Russia. *Journal of Geophysical Research: Solid Earth*, *130*, e2025JB032561. https://doi.org/10.1029/2025JB032561

Received 1 AUG 2025
Accepted 24 OCT 2025

Author Contributions:
Conceptualization: S. Scheidt
Data curation: S. Scheidt, J. I. Svendsen, H. Haflidason
Formal analysis: S. Scheidt, S. Ólafsdóttir, J. Brendryen, N. R. Nowaczyk, M. M. Lenz
Funding acquisition: S. Scheidt, J. I. Svendsen, H. Haflidason
Investigation: S. Scheidt
Methodology: S. Scheidt, S. Ólafsdóttir, J. Brendryen
Project administration: J. I. Svendsen, H. Haflidason
Resources: J. I. Svendsen, H. Haflidason
Software: N. R. Nowaczyk
Validation: S. Scheidt
Visualization: S. Scheidt
Writing – original draft: S. Scheidt

New Insights Into the Proposed Geomagnetic Excursion Hilina Pali From High-Resolution Lake Sediment Cores From the Polar Ural Mountains, Arctic Russia

S. Scheidt[1], S. Ólafsdóttir[2,3], J. Brendryen[2], N. R. Nowaczyk[4], M. M. Lenz[1], J. I. Svendsen[2], and H. Haflidason[2]

[1]University of Cologne, Institute for Geology and Mineralogy, Cologne, Germany, [2]Department of Earth Science, University of Bergen, Bergen, Norway, [3]Reykjavík Energy, Reykjavík, Iceland, [4]GFZ Helmholtz Centre for Geosciences, Section 2.3 Geomagnetism, Potsdam, Germany

Abstract This study presents paleomagnetic records from three 24 m-long sediment cores from the neighboring lakes Bolshoye Shchuch'ye and Maloye Shchuch'ye, located about 10 km apart in the Polar Urals in northern Russia. The age model, based on radiocarbon dating and varve counting, shows that the sediment sequences reach back up to about 23.5 ka cal. BP. Mineral magnetic analyses indicate that the upper sedimentary sequence is not suitable for paleomagnetic analyses. Below about 6.7 m the paleosecular variation and relative paleointensity in the magnetic field in the period 23.6–14.8 ka cal. BP is reconstructed. The magnetostratigraphic results show very similar pattern in both lakes including a directional anomaly previously called the Bolshoye Shchuchye Event. This event is dated to the period 20.2–19.1 ka cal. BP accompanied with a low in relative paleointensity. Comparisons with sediment records from other regions suggest that this paleomagnetic feature represents the proposed Hilina Pali geomagnetic excursion, which is documented in unprecedented high resolution in the studied lakes. The reconstructed path of the virtual geomagnetic field during this event shows that the pole positions remain at latitudes higher than 55°N while describing a clockwise loop. According to varve counts the inclination deviation and virtual geomagnetic pole latitude deviation associated with Hilina Pali lasted 1135 ± 35 years and 1294 ± 44 years, respectively, in northern Russia.

Plain Language Summary This study examines three sediment cores taken from the two lakes Bolshoye Shchuch'ye and Maloye Shchuch'ye, in the Polar Ural Mountains in northern Russia. The analyses were carried out to determine the direction and intensity of the Earth's magnetic field during sediment deposition, as recorded by magnetic minerals. The ages of the various layers were determined using dating methods such as radiocarbon dating and counting annual layers (varves). The core sections between 23.5 and 6.7 m correspond to an age between 23,600 and 14,800 years. During this period, both lakes recorded very similar paleomagnetic information, including an anomaly previously called the Bolshoye Shchuchye Event. Comparisons with other records show that this event corresponds to the earlier proposed Hilina Pali geomagnetic excursion. According to our study, Hilina Pali occurred between approximately 19,000 and 20,300 years ago and was accompanied by low intensity of the geomagnetic field. However, because the magnetic pole positions remain at latitudes higher than 55°N Hilina Pali does not meet the criteria for classification as a geomagnetic excursion. This study provides a rare data set of high-resolution sediment from the high North that is important to better understand how Earth's magnetic field changed over time.

1. Introduction

Geomagnetic excursions are classically defined as times when the position of the virtual geomagnetic pole (VGP) deviates by at least 40–45° from the geographic pole (Merrill & McFadden, 1994; Verosub & Banerjee, 1977) while the relative paleointensity (RPI) of the Earth's magnetic field shows a minimum (Laj & Channell, 2007). It is, however, an ongoing debate whether geomagnetic excursions are global features and occur synchronously worldwide. Over time, a large number of putative geomagnetic excursions were proposed, but only a few of them were finally accepted as well-documented instabilities of the geomagnetic field with acceptable age control (e.g., Channell et al. (2020), and references therein). Today, the youngest of them is the one first discovered at Mono Lake, which occurred about 34 ka ago (e.g., Liu et al., 2020). However, further, more recent geomagnetic excursions are postulated. One of these is Hilina Pali, which was first documented in lava flows in Hawaii by Coe et al. (1978) and dated to ~19 ka. Over the decades Hilina Pali has been associated with findings in different

Writing – review & editing: S. Scheidt, S. Ólafsdóttir, J. Brendryen, N. R. Nowaczyk, M. M. Lenz, J. I. Svendsen, H. Haflidason

geological archives. In addition to snapshots documented in volcanic rocks (see compilation in Liu et al., 2020; Leonard et al., 2017; Laj et al., 2002; Teanby et al., 2002), Hilina Pali has been suggested to be documented in sedimentary deposits across the globe (Table 1). In addition, field instabilities between 17 ka and 22 ka were identified in other sediment sequences, which could also represent Hilina Pali (e.g., Brandt et al., 1999; Clark & Kennett, 1973; Laj et al., 2014; Lund et al., 1988; Nowaczyk et al., 2003; Nowaczyk & Knies, 2000; Peck et al., 1996).

Despite the successively increasing number of studies, the validation of Hilina Pali as a globally recognizable geomagnetic excursion has been hampered so far by the still overall small number of recordings and large inconsistencies in terms of timing and duration. In addition, the extent of field deviation also varies throughout the studies, some report reversed or transitional directions–others that the VGP latitudes remained higher than 60°N. To resolve the question on the timing, duration, and characteristics of Hilina Pali, further high-resolution recordings are needed. Sediment archives are particularly important for this purpose, as only these can potentially provide very detailed and continuous information on the occurrence and magnitude of fluctuations of the intensity and direction of the Earth's magnetic field.

Here we report results from paleomagnetic investigations of high-resolution sediment cores that were retrieved from the two neighboring lakes Bolshoye Shchuch'ye (озеро Большое Щучье; hereafter Bol.S.) and Maloye Shchuch'ye (озеро Малое Щуч; hereafter Mal.S.), located in the Polar Ural Mountains in northern Russia (Figure 1). Sediment cores from these lakes have previously been the subject of several investigations including sediment stratigraphy, geochronology, paleoenvironment and glacial history (Bjune et al., 2022; Clarke et al., 2020; Haflidason, Regnéll, et al., 2019; Haflidason, Zweidorff, et al., 2019; Regnéll et al., 2019; Svendsen et al., 2019). Furthermore, Haflidason et al. (2022) reported anomalies in the paleomagnetic inclination records from both lake basins in the time interval 20.5–19.2 ka cal. BP, which they referred to as the Bolshoye Shchuchye Event. Since neither magnetic carriers were analyzed nor declination data were available, no attempt was made to compare the records with known paleomagnetic records from other regions. Here we present an updated and more thoroughly processed data set that includes analyses of magnetic mineralogy, the magnetic secular variation (PSV), VGP path, and relative paleointensity (RPI).

2. Study Site

The lakes Bol.S. and Mal.S. are located about 10 km apart in the Russian Arctic (Figure 1). Both lakes were formed by glacial erosion in north-west to south-east oriented valleys. The bedrock of the surrounding 800–1,200 m high peaks of the Ural Mountains consists of basaltic and andesitic rocks from the Proterozoic and Cambrian in the east and north-west: Ordovician quartzites and phyllites outcrop in the south and west of the lakes (Dushin et al., 2009). With a length of 12.8 km, a width of around 1 km, and a water depth of up to 140 m, Lake Bol.S. is the largest and deepest lake in the Polar Ural Mountains. Its lake level is 187 m above sea level and its catchment area is about 215 km^2 wide. The lake is mainly fed by streams flowing from the mountains in the north-west and it drains into the Shchuch'ye River (Малая Щучья) in the south-east. Bathymetric mapping and seismic profiling revealed that the lake hosts a 160 m thick sediment sequence in its central part (Haflidason, Zweidorff, et al., 2019). Lake Mal.S. is the second largest lake in the Polar Urals. It is 7.15 km long, about 0.6 km wide and has a maximum water depth of approximately 40 m. Its lake level is at 287 m above sea level, and the catchment area covers about 51 km^2. The main inflow into Lake Mal.S. comes from the mountain ranges to the south-west and from the mountains to the north-west, which also shelter a tiny remnant of a glacier (Svendsen et al., 2019). Like Lake Bol.S., Lake Mal.S. drains to the south-east into the Shchuch'ye River that eventually flows down to the West Siberian lowland in the east.

3. Material and Methods

3.1. Core Recovery and Sample Preparation

Cores from both lakes were recovered with an UWITEC piston corer using 200 cm long liners with a 9 cm diameter in 2009 (Svendsen et al., 2019). Only the material of the lowermost run of core 506-50 was recovered in a stainless-steel barrel. Due to the coring procedures, the individual core sections are randomly orientated in respect to the azimuth and interrupted by ≤10 cm gaps from core catchers. With the intention of obtaining the entire sediment sequence of lake Bol.S., two parallel cores (506-48 and 506-50) were retrieved at about 20 m from each other and with a slight offset in depth for each two-m-long core section. The two cores were recovered from

Table 1
Overview on Studies Documenting Hilina Pali and Its Chronology in Sedimentary Archives

Site	Archive type	Age or duration (ka)	Dating Method (s)	Reference
Black Sea (Türkiye)	Marine	~18.5	AMS^{14}C, lith. (AMS^{14}C), NGRIP	Liu et al. (2018)
Sea of Marmara (Türkiye)	Marine	~18	AMS^{14}C, tephra, NGRIP	Makaroğlu et al. (2020)
Equatorial Pacific (Papua New Guinea)	Marine	~18.5	AMS^{14}C	Dauchy-Tric et al. (2024)
Lake Baikal (Russia)	Lacustrine	~20	AMS^{14}C	Peck et al. (1996)
Laguna Potrok Aike (Argentina)	Lacustrine	~20	AMS^{14}C, tephra	Lisé-Pronovost et al. (2013)
Heqing Basin (China)	Lacustrine	~17	AMS^{14}C, RPI(PISO)	Xu et al. (2024)
Lake Challa (Kenia)	Lacustrine	19.3–21.5	lith. (AMS^{14}C/^{210}Pb)	Di Chiara et al. (2025)
Jeju Islan (Korea)	Terrestrial (wetlands)	17.6–18.8 and ~20.2	AMS^{14}C, RPI(PISO)	Ahn et al. (2018)
Western Ukraine	Terrestrial (loess)	~18	OSL	Nawrocki et al. (2018)

Note. If no clear duration is stated, midpoint event ages are provided. Dating methods are abbreviated as follows: AMS^{14}C = accelerator mass spectrometry radiocarbon dating, lith (AMS^{14}C) = lithostratigraphic correlation to AMS^{14}C dated layers, lith (AMS^{14}C/^{210}Pb) = lithostratigraphic correlation to the AMS^{14}C and ^{210}Pb dated layers, NGRIP = correlation of XRF data to the NGRIP δ^{18}O ice core record, OSL = optically stimulated luminescence, RPI(PISO) = RPI correlation to the PISO-1500 global RPI stack (Channell et al., 2009), tephra = tephra stratigraphy or geochemical fingerprinting of tephra. Please note, Ahn et al. (2018) suggest multiple excursional swings which are reflected by the two entries.

the southern part of Lake Bol.S. (67°51.37′N, 66°21.50′E) from a water depth of about 100 m and cover a total sediment thickness of about 24 m. An equally long core (506-51) was obtained from the middle part of Lake Mal. S. (67°49.10°N, 66°09.70°E) where the water depth is about 30 m. In the sediment laboratory at the University of Bergen (Norway), all core segments (i.e., the individual liners) were cut into about 1-m-long sections and split lengthwise. For magnetic analyses, u-channels with an inner size of 2 × 2 cm were sampled. The lowermost two m of core 506-50 was not sampled for u-channel measurement because it was retrieved in a steel barrel that was opened using a cutting burner. Due to the high risk that this process may have altered the magnetic signal this core segment was not considered for this study. Further details on coring equipment, core handling, and sampling procedures are described by Haflidason, Regnéll, et al. (2019) and Haflidason et al. (2022). As only the composite depth of cores 506-48 and 506-50 were reported in previous publications and the depth scale of 506-51 was adjusted to this composite depth, an individual depth scale of all cores is introduced in this study. We place the base of each core segment at the target depth of the individual coring runs. An exception was made for one incomplete core segment of core 506-50, where the correlation to core 506-48 was determined by visual correlation of the strata. To account for sediment expansion, we compressed the length of all core segments longer than 190 cm to a length of 190 cm.

Information on magnetic mineralogy was gained from about 300 mg lyophilized sediment material compressed in gel capsular samples from 85 selected depth levels of core 506-48. Furthermore, magnetic minerals were extracted from 12 of the 85 samples. For this purpose, the remaining lyophilized sample material (2–10 g) was dispersed in demineralized water and circulated for at least an hour through tubes passing strong magnets. After completion of the circulation process, the magnetically captured material in the tubes, was rinsed, cleaned with ultrasound and then dried.

3.2. Sediment Material

The sedimentary sequences of the cores from both lakes can be divided into three main lithological units, labeled A, B, and C (Eldegard, 2019; Regnéll et al., 2019; Svendsen et al., 2019). The lowermost unit C consists of well-defined, 1–5 mm thick rhythmic layers, consisting mainly of fine silt and clay. These layers are identified as annual varves (Regnéll et al., 2019). The overlying unit B starts at about 11.5 m core depth and shows a more

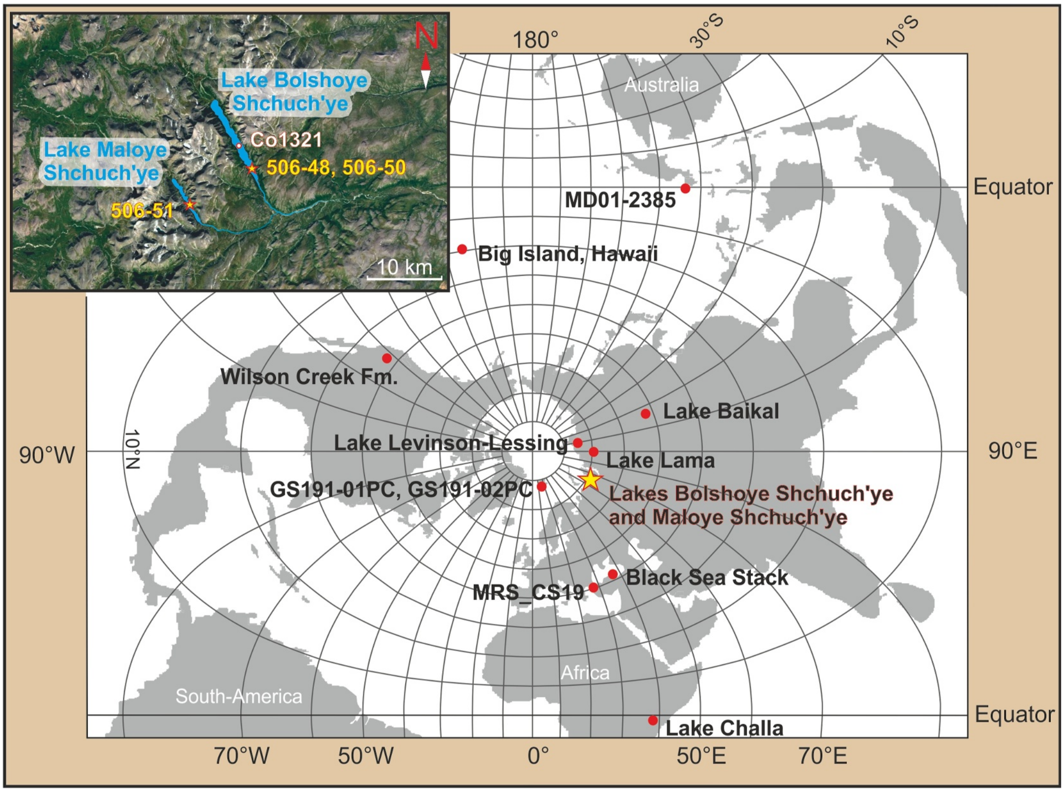

Figure 1. Transverse spherical Mercator projection including all cores and sites discussed in this study (red dots) and the location of the lakes Bol.S. and Mal.S. (yellow star). The satellite picture shows the lakes Bol.S. and Mal.S. and the locations of the drill sites (Earth google, 2025). The site location of core Co1321 (Lenz et al., 2022) is shown for comparison.

diffuse and discontinuous layering that alternates with nearly homogeneous sediments. The topmost unit A comprises 6.64 m of the core. It consists mainly of homogeneous sediments intercalated by several thin turbidites of fine sand or silt. The frequency of turbidites is higher in Lake Mal.S. than in Lake Bol.S.. In the latter lake, the sediments of units C and B are characterized by an almost homogeneous sediment sequence consisting of fine to medium-sized silt (mean D50 = 8 μm) and a relatively low organic carbon content with a value of loss on ignition (LOI) of 2.5%–3.5%. Unit A is a little coarser grained (mean D50 = 10.25 μm) and has a slightly higher LOI values of 3.5%–4.5% (Eldegard, 2019).

3.3. Rock and Paleomagnetic Analyses

The magnetic susceptibility and the magnetic remanence of u-channels were measured at the Paleomagnetic and Environmental Magnetic Research Laboratory, College of Earth, Ocean, and Atmospheric Sciences, Oregon State University (USA) at 1-cm intervals. The u-channel magnetic susceptibility (κ_{rel}) of cores 506-48 and 506-50 were obtained using a motion-controlled u-channel track built at Oregon State University equipped with a Bartington MS-meter and a MS2C loop sensor with an internal diameter of 36 mm. The remanence measurements were conducted using a model 755-1.65UC 3-axis superconducting rock magnetometer (2G Enterprises, USA) optimized for u-channel samples (Oda et al., 2016; Oda & Xuan, 2014). The measurements of the natural remanent magnetization (NRM) of all three cores were followed by 14 stepwise increasing alternating field (AF) demagnetization steps up to 80 mT (10, 15, 20, 25, 30, 35, 40, 45, 50, 55, 60, 65, 70, 80 mT). For few core segments also 90 and/or 100 mT were applied. Subsequently, an anhysteretic remanent magnetization (ARM) with a peak AF field of 100 mT and a direct current bias field of 0.05 mT was imparted to cores 506-48 and 506-50. The ARM measurement was followed by AF demagnetization in the same steps as used for NRM demagnetization. Finally, only core 506-48 was given an isothermal remanent magnetization (IRM) with a field of 1 T, which was also demagnetized with the same steps as the NRM. All obtained data was initially checked and corrected for offsets and flux jumps using the UPmag software (Xuan & Channell, 2009). Remanence data from

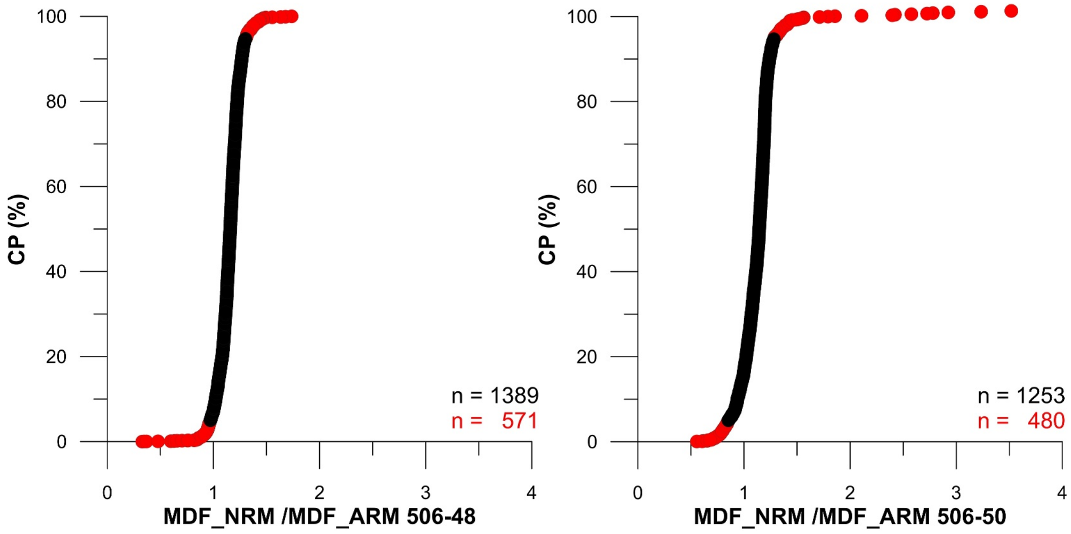

Figure 2. MDF_{NRM}/MDF_{ARM} ratio against the cumulative percentage of cores 506-48 and 506-50. Data points shown in red were excluded from the RPI determination.

disturbed sections and turbidites (see Scheidt et al., 2025) were generally excluded. Due to the response curve of the measuring device (Oda & Xuan, 2014), data from the 5 cm adjacent to disturbances and from the ends of core sections were also not included in this study.

The characteristic remanent magnetization (ChRM) was determined by principal component analysis (Kirschvink, 1980) with the Puffin Plot software (Lurcock & Wilson, 2012) by using the seven consecutive AF demagnetization steps between 30 and 60 mT without anchoring to the origin. The six levels between 45 and 100 mT were only used for core segment 12-1 of core 506-51, as levels 30 and 60 mT were inadvertently not available. Parts of the cores with maximum angular deviation (MAD) values >5° were excluded from the analyses because they are assumed to be indicative for core disturbances and deformation. The ChRM declinations were aligned to the neighboring core segments. Subsequently the VGP was determined from the local inclination and declination values.

The relative paleointensity (RPI) proxy was determined by using the partial NRM normalized by the partial ARM, and, if available, partial IRM (Tauxe et al., 1995). Partial refers to the demagnetization steps between 30 and 60 mT. The median destructive field (MDF) of the NRM and the ARM were determined using the PuffinPlot software. To ensure the normalizer activates the same magnetic assemblage that is responsible for the NRM acquisition, all samples whose MDF_{NRM}/MDF_{ARM} ratio against the cumulative frequency deviated from a linear trend were excluded from the RPI record (Figure 2). This implies that measurements from depth intervals that did not reach the MDF point were also discarded.

Isothermal remanent magnetization acquisition curves, IRM backfield curves, and hysteresis loops were obtained from gel-capsular samples using a model 8604 vibrating sample magnetometer (Lakeshore, USA) in the Rock and magnetic Laboratory of the University of Cologne (Germany). The hysteresis loops and IRM backfield curves were measured up to 1.8 T. For magnetic granulometry, hysteresis measurements were started with the M_{si} curves (Fabian & von Dobeneck, 1997) to provide evidence on the proportion of multi-domain (MD) particles (Fabian, 2003). Hysteresis measurements were corrected for pole saturation before the saturation magnetization (M_s) was calculated using the approach to saturation model of (Fabian, 2006). The saturation remanence M_{rs} and coercive force H_c was determined from the intersections of the hysteresis with the magnetization axis and field axis, respectively. The coercivity of remanence H_{cr} was obtained from the backfield of remanence curve by linear interpolation.

Temperature-dependent magnetic susceptibility (κ_T) was determined on magnetic extracts with kaolin as filler and have been performed at the University of Cologne with the MFK2-FA Kappabridge (AGICO, Czech Rep.). The measurements included heating and cooling runs between 40°C and 700°C (medium speed) at a frequency of

976 Hz and 200 A/m field intensity in argon atmosphere. The Curie Temperature (T_C) was approximated by linear fits of the steep slopes in the inverse susceptibility (Petrovský & Kapička, 2006).

3.4. Chronology and Correlation

The chronology of lake Bol.S. is based on 38 previously published accelerator mass spectrometry radiocarbon (AMS ^{14}C) ages, the Vedde Ash (12.1 ka cal. BP, Lohne et al., 2013), and varve-counts (Haflidason et al., 2022; Haflidason, Regnéll, et al., 2019; Regnéll et al., 2019; Svendsen et al., 2019). This study uses the same data (Table 2), but it has been processed slightly differently to construct an updated age-depth model for core 506-48 (Scheidt et al., 2025). All AMS^{14}C ages are calibrated using the OxCal 4.4.1 software (Ramsey, 2009a) with IntCal20 calibration curve (Reimer et al., 2020). The model is constructed using the P_Sequence deposition model (Ramsey, 2008) and the variable *k* option (Ramsey & Lee, 2013). The age of the Vedde Ash was updated with the IntCal20 calibration curve. However, this time, several thin turbidites between 0.4 and 2.6 cm (in sum 87.9 cm) previously identified by Regnéll et al. (2019) were inserted as instantaneous events in the depositional model (Scheidt et al., 2025). Boundary commands were inserted at transitions between sediment units where the sedimentation rates are likely to have changed. The general outlier model (Ramsey, 2009b) is used to assess the probability of each AMS^{14} C date for being an outlier (Table 2). A prior outlier probability of 5% is applied for most dates, except for two dates in the varved intervals that were considered outliers by (Haflidason et al., 2022). These dates are omitted in the present age model. In the varved interval, the number of counted varves and the associated uncertainties are included as a normally distributed interval between each AMS^{14}C date.

The age model of core 506-48 is transferred to core 506-50 using tie-points derived from a total of 125 visually identified features in color images (Scheidt et al., 2025). Core 506-51 is correlated to 506-48 using five of the AMS^{14}C dates from the upper 4.65 m of core 506-51 (Haflidason et al., 2022) and 34 tie points based on correlation of ChRM directions (Scheidt et al., 2025). Correlation and age transformation was performed using the software QAnalySeries (Kotov & Paelike, 2018).

4. Results

4.1. Magnetic Mineralogy

The cores from lakes Bol.S. and Mal.S. are characterized by relatively high NRM, ARM and IRM intensities and relatively high κ_{rel} values (Table 3, Figure 3). Based on the u-channel measurements of core 506-48, two mineral magnetic units can be distinguished (Figures 3 and 4). The boundary at 6.68 m depth corresponds almost with the transition of the lithological units B and A at 6.64 m defined by Regnéll et al. (2019). The variability of the measurement results and the parameters determined by them is significantly lower in the lower parts of the cored sequence of Lake Bol.S. than in their upper parts or in the measurements from the sequence in Lake Mal.S. (Figure 3).

The residual magnetization after AF demagnetization is remarkably high in all measurements. Even in the final data set used (i.e., after excluding samples for various reasons), the cores show high median percentages of residual NRM: core 506-51 yielded 31% and 33% in the lower and upper mineral magnetic units, respectively; cores 506-48 and 506-50 yielded values of 27% and 22% in the lower part and 36% and 28% in the upper part, respectively. Accordingly, the sediments contain both soft and hard magnetic components, and variations in the mineral magnetic composition, concentration, and the domain state of the magnetic minerals are smaller in the lower parts of the sequence from Lake Bol.S. than in its upper parts and in Lake Mal.S. (Figures 4a–4e). A decrease in concentration-sensitive parameters toward the top with minimum values between 2 and 4 m (peak Holocene) coincide with the phase of probably higher biological productivity in Lake Bol.S. (Regnéll et al., 2019). These observations suggest that detrital magnetic minerals might have been dissolved during the Holocene when suboxic conditions caused by bacterial decomposition of organic matter prevailed. This effect has also been observed in the Siberian lake Levinson-Lessing (Scheidt et al., 2022).

Hysteresis measurements of all samples from the sediment succession also reflect the presence of high-coercivity minerals. Because the samples were exposed to a field of 1.8 T before the field direction was reversed, the openness of the loop in fields >1 T (Figure 5a) proves that a small portion of the magnetization at each measurement point is carried by minerals whose coercivity of remanence (H_{cr}) is higher than the applied field strength. The hysteresis parameters coercivity force (H_c) and H_{cr} show quite stable values below about 10 m and a gradual

10.1029/2025JB032561

Table 2
Dating Results From Core 506-48 From Indicated Studies Used to Calculate the Age Model as Described in the Study

Lab_Id	506-48 core depth (cm)	Conventional ^{14}C ages (yr.) ^{14}C years	Conventional ^{14}C ages (yr.) 1σ	Calibrated ^{14}C ages (yr cal. BP) Mean	Calibrated ^{14}C ages (yr cal. BP) 1σ	Taken from (reference)	Outlier probability (%) Prior	Outlier probability (%) Posterior	Outlier model	Type
Poz-79407	24.5	1,480	30	1,355	27	Svendsen et al. (2019)	5	1	General	t
Poz-69670	85.0	2,285	30	2,275	63	Svendsen et al. (2019)	5	1	General	t
Poz-79408	131.0	2,645	35	2,768	30	Svendsen et al. (2019)	5	1	General	t
Poz-79409	190.5	3,730	35	4,075	63	Svendsen et al. (2019)	5	1	General	t
Poz-69671	219.7	4,565	35	5,220	104	Svendsen et al. (2019)	5	2	General	t
Poz-79410	272.2	5,890	40	6,712	49	Svendsen et al. (2019)	5	1	General	t
Poz-69673	359.7	7,750	60	8,521	65	Svendsen et al. (2019)	5	1	General	t
Poz-79412	444.8	9,700	70	11,048	137	Svendsen et al. (2019)	5	2	General	t
Poz-79413	479.1	10,010	50	11,505	124	Svendsen et al. (2019)	5	2	General	t
LuS14118	486.1	10,250	50	11,982	150	Haflidason et al. (2022)	5	20	General	t
LuS14119	509.7	10,120	50	11,696	129	Haflidason et al. (2022)	5	11	General	t
Vedde Ash	518.9			12,049	47	Haflidason et al. (2019a, 2019b)				
LuS14120	523.4	10,510	50	12,520	115	Haflidason et al. (2022)	5	10	General	t
Beta-282484	560.2	10,560	50	12,583	76	Svendsen et al. (2019)	5	1	General	t
LuS14121	577.6	10,650	65	12,651	67	Haflidason et al. (2022)	5	4	General	t
LuS14122	581.6	11,090	60	12,998	69	Haflidason et al. (2022)	5	2	General	t
LuS14123	589.6	11,380	60	13,255	60	Haflidason et al. (2022)	5	1	General	t
LuS14124	592.5	11,410	60	13,281	67	Haflidason et al. (2022)	5	0	General	t
LuS14125	599.5	11,480	75	13,354	78	Haflidason et al. (2022)	5	1	General	t
LuS14126	624.3	11,900	60	13,758	109	Haflidason et al. (2022)	5	1	General	t
Beta-473333	632.2	12,310	40	14,330	204	Svendsen et al. (2019)	5	75	General	t
Beta-473334	632.2	12,040	40	13,917	70	Svendsen et al. (2019)	5	25	General	t
LuS14127	659.7	12,480	75	14,670	213	Haflidason et al. (2022)	5	1	General	t
Unit A/B Boundary	664.0					Regnéll et al. (2019)				
LuS14128	670.5	12,520	75	14,749	216	Haflidason et al. (2022)	5	1	General	t
Beta-282485	727.2	12,700	50	15,143	81	Svendsen et al. (2019)	5	1	General	t
Beta-473335	792.6	13,020	50	15,589	98	Svendsen et al. (2019)	5	2	General	t
Poz-79403	876.9	14,300	140	17,446	228	Svendsen et al. (2019)	5	29	General	t
Poz-69674	968.5	14,390	100	17,572	171	Svendsen et al. (2019)	5	2	General	t
Poz-69675	1,108.4	15,030	130	18,410	162	Svendsen et al. (2019)	5	1	General	t
Unit B/C Boundary (top varve count)	1,147.9					Regnéll et al. (2019)				
Poz-69677	1,181.5	15,660	90	18,943	87	Svendsen et al. (2019)	5	1	General	t

10.1029/2025JB032561

Table 2
Continued

Lab_Id	506-48 core depth (cm)	Conventional ^{14}C ages (yr.)		Calibrated ^{14}C ages (yr cal. BP)		Taken from (reference)	Outlier probability (%)		Outlier model	Type
		^{14}C years	1σ	Mean	1σ		Prior	Posterior		
Beta-282486	1,295.5	15,180	60	18,466	115	Svendsen et al. (2019)	5	100	General	t
Poz-69678	1,539.4	17,620	150	21,340	253	Svendsen et al. (2019)	5	100	General	t
Poz-79414	1,723.0	17,400	150	21,045	222	Svendsen et al. (2019)	5	1	General	t
Poz-79404	1,938.0	18,370	210	22,303	242	Svendsen et al. (2019)	5	8	General	t
Poz-79405	2,064.0	16,700	170	20,168	221	Svendsen et al. (2019)	5	100	General	t
Poz-69680	2,346.4	20,380	120	24,504	192	Svendsen et al. (2019)	5	100	General	t
Poz-79406	2,346.4	18,750	170	22,684	170	Svendsen et al. (2019)	5	92	General	t
Base of core (base varve count)	2,370.0			22,000	2,286	Regnéll et al. (2019)				

Note. Depth is given in the individual depth of core 506-48 used in this study. Dates supporting the varve chronology are highlighted in gray. Entries not related to AMS^{14}C-dating have no outlier probability. Further details on the data are provided by Haflidason et al. (2022) and in the references therein.

Table 3
Maximum (Max), Minimum (Min), Median (Med) and Percentiles of 95, 75, 25, 5 of NRM (mA/M), MDF of NRM (mT), κ_{rel} (E-6), ARM (mA/m), IRM (mA/m) of the U-Channel Measurements of the Individual Cores

		NRM			MDF_{NRM}			κrel		ARM		IRM
		506-48	506-50	506-51	506-48	506-50	506-51	506-48	506-50	506-48	506-50	506-48
Upper unit	Max	3.535	2.357	2.108	98.50	72.50	96.40	227.0	245.3	2.249	1.579	114.904
	95%	2.415	2.039	1.912	73.90	62.72	80.21	210.0	211.6	1.675	1.430	111.250
	75%	1.716	1.400	1.316	62.40	56.00	63.95	153.0	160.2	1.339	1.107	81.983
	Med	1.123	1.051	0.836	57.20	53.10	57.20	107.0	94.2	0.928	0.851	59.445
	25%	0.809	0.852	0.632	54.10	47.68	51.78	76.8	77.2	0.728	0.730	48.653
	5%	0.587	0.482	0.414	48.96	43.40	32.59	56.7	57.6	0.557	0.512	38.762
	Min	0.354	0.356	0.340	43.30	41.20	10.90	33.7	15.2	0.490	0.367	36.534
Lower unit	Max	2.918	2.585	3.624	65.60	51.30	98.00	274.0	249.3	1.696	1.736	119.388
	95%	1.817	1.842	2.435	47.00	45.83	79.51	210.0	199.7	1.489	1.341	108.857
	75%	1.388	1.458	1.989	42.60	41.40	61.60	196.0	187.8	1.329	1.222	101.008
	Med	1.217	1.324	1.656	40.90	39.30	52.90	188.0	179.3	1.244	1.158	95.638
	25%	1.072	1.155	1.360	39.30	38.00	47.40	179.0	172.7	1.176	1.094	90.563
	5%	0.868	0.936	1.064	37.40	35.40	38.65	163.0	161.9	1.038	0.987	81.746
	Min	0.472	0.731	0.746	34.60	33.50	32.20	85.3	127.0	0.925	0.845	74.515

Note. The values only reflect measurements that were considered for PSV analyses. The boundary between the lower and upper units lies at a depth of 6.68 m.

increase above. In contrast, the remanent magnetization (M_{rs}) and the saturation magnetization (M_s) are stable within a narrow range and show only an insignificant decreasing trend in the uppermost few meters (Figures 4e and 4f). Since the ferrimagnetic mineral components are supplemented by minerals with high coercivity, it is no longer recommended to use the Day diagram (Day et al., 1977) as a magnetic domain size indicator (Roberts et al., 2019). However, if we assume that the high-coercivity components mainly push the H_c/H_{cr} ratios to higher values (e.g., Scheidt et al., 2017), the Day plot indicates either dominance of single vortex (SV) and multi vortex (MV) domain states with axial ratios between 1 and 2, or a mixture of SD and MD particles (Williams et al., 2024).

For closer evaluation of the magnetic granulometry, hysteresis measurements started with M_{Si} curves. The areas enclosed by the initial saturation curve and the upper branch of the hysteresis loops $\left(E_t^{\Delta}/2\right)$ accounts for <3% of the total area E_{hys} of most individual hysteresis loops (Figure 5b). However, it was not possible to specify the exact ratio E_t^{Δ}/E_{hys} without unacceptable large errors, as tiny gaps are present between the upper and lower branches (Figure 5c). As stated above, this is probably caused by the high coercive component, although a slight drift in the measurement may also have an influence. Nevertheless, the little size of $E_t^{\Delta}/2$ compared to the complete area of the hysteresis in all measurements can be visually identified and indicate that MD particles have a small proportion within the mineral magnetic composition (Fabian, 2003). Thus, the dominance of SV and MV domain states likely yield to the result in the Day plot.

The identification of the ferrimagnetic mineral constituents is performed by κ_T measurements of magnetic extracts. Two similar sets of irreversible curves can be distinguished: measurements from the upper five samples (Figure 4g) and the lower seven samples (Figure 4h). Accordingly, two samples from the lower mineral magnetic unit (from 7.14 to 9.19 m) are more like the κ_T path of the samples from the upper unit than from the lower unit. In all measurements, the identified minerals are essentially the same: the increase in the heating runs until a weak maximum at around 300°C is related to the presence of maghemite (e.g., Banfield et al., 1994). This mineral likely results from low-temperature oxidation of magnetite which is less intense in the younger part of the sediment succession. Some samples show a second, more or less wide maximum between 450 and 500°C, which is interpreted to indicate titanomaghemite that exsolves to magnetite and ilmenite above around 300°C (Özdemir, 1987). The subsequent decrease reveals the presence of low-Ti titanomagnetites. Only the sample from 3.25 m shows a weak Hopkinson peak, which also supports the interpretation that most ferrimagnetic minerals are in the SV or MV domain state. The major drop at temperatures between 579°C and 602°C is due to partially oxidized

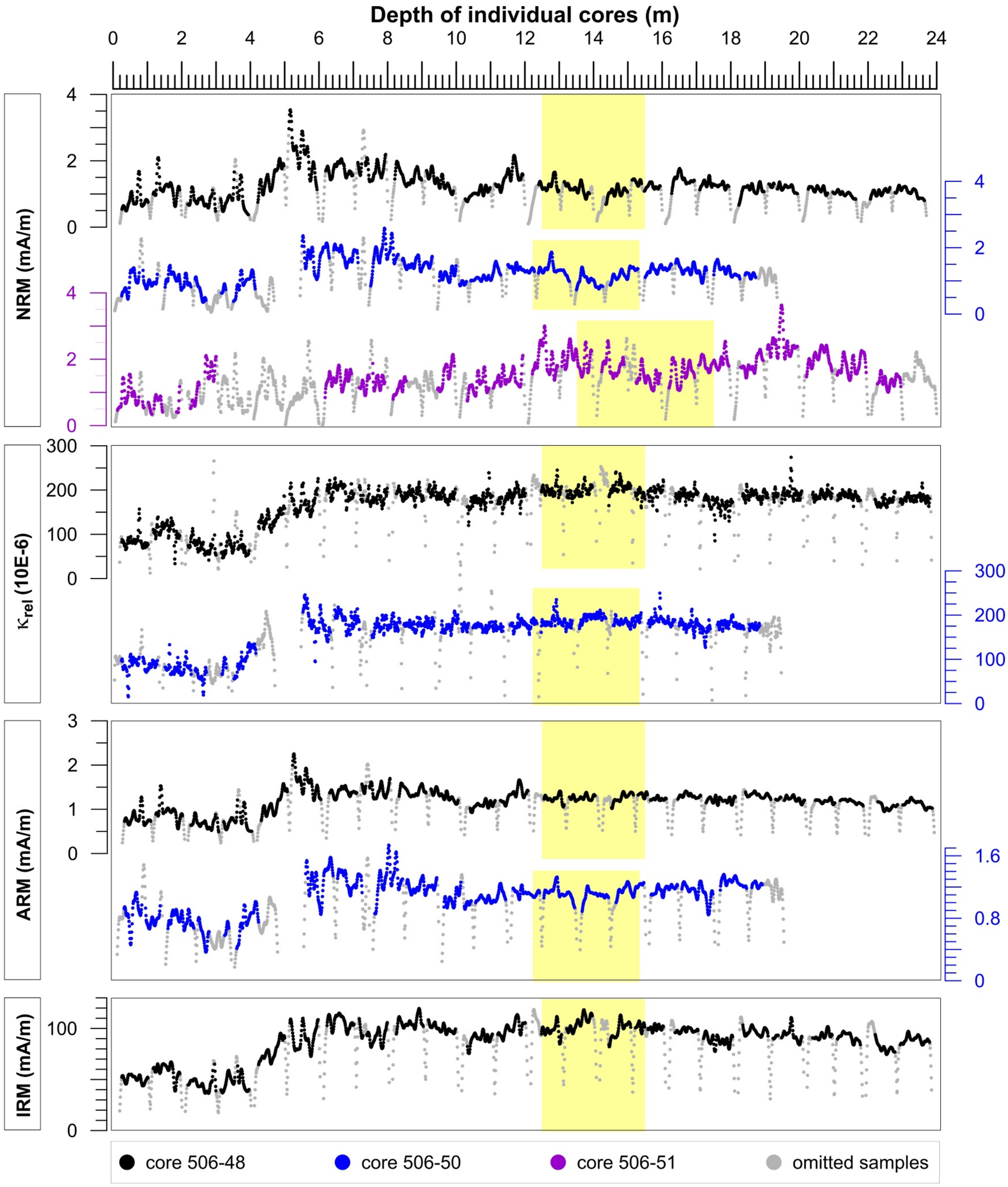

Figure 3. Downcore data for comparison: natural remanent magnetization, κ_{rel}, anhysteretic remanent magnetization, and isothermal remanent magnetization from cores 506-48 (black), 506-50 (blue), and 506-51 (purple) versus individual core depths. Discarded values of all cores are shown in gray. The yellow marked depth intervals refer to the time periods highlighted in Figures 7 and 9.

magnetite (Gehring et al., 2009; Muxworthy et al., 2023). The small maximum between 600°C and 700°C indicates a temperature induced formation of a mineral phase, which is not relevant for the identification of the primary magnetic mineral assemblage. Due to progressive thermal inversion and structural effects, the cooling curves show a somewhat higher T_C of magnetite and often slightly higher intensities than the heating curves. This can be explained by the formation of magnetite from titanomaghemite as described above. As hematite and goethite are antiferromagnetic and the magnetic extraction process favors ferrimagnetic minerals, the role of hematite and goethite in the magnetic mineralogy cannot be assessed from the magnetic extracts. However, the high residual magnetization after AF treatment suggests that high coercivity minerals are also present. Since this

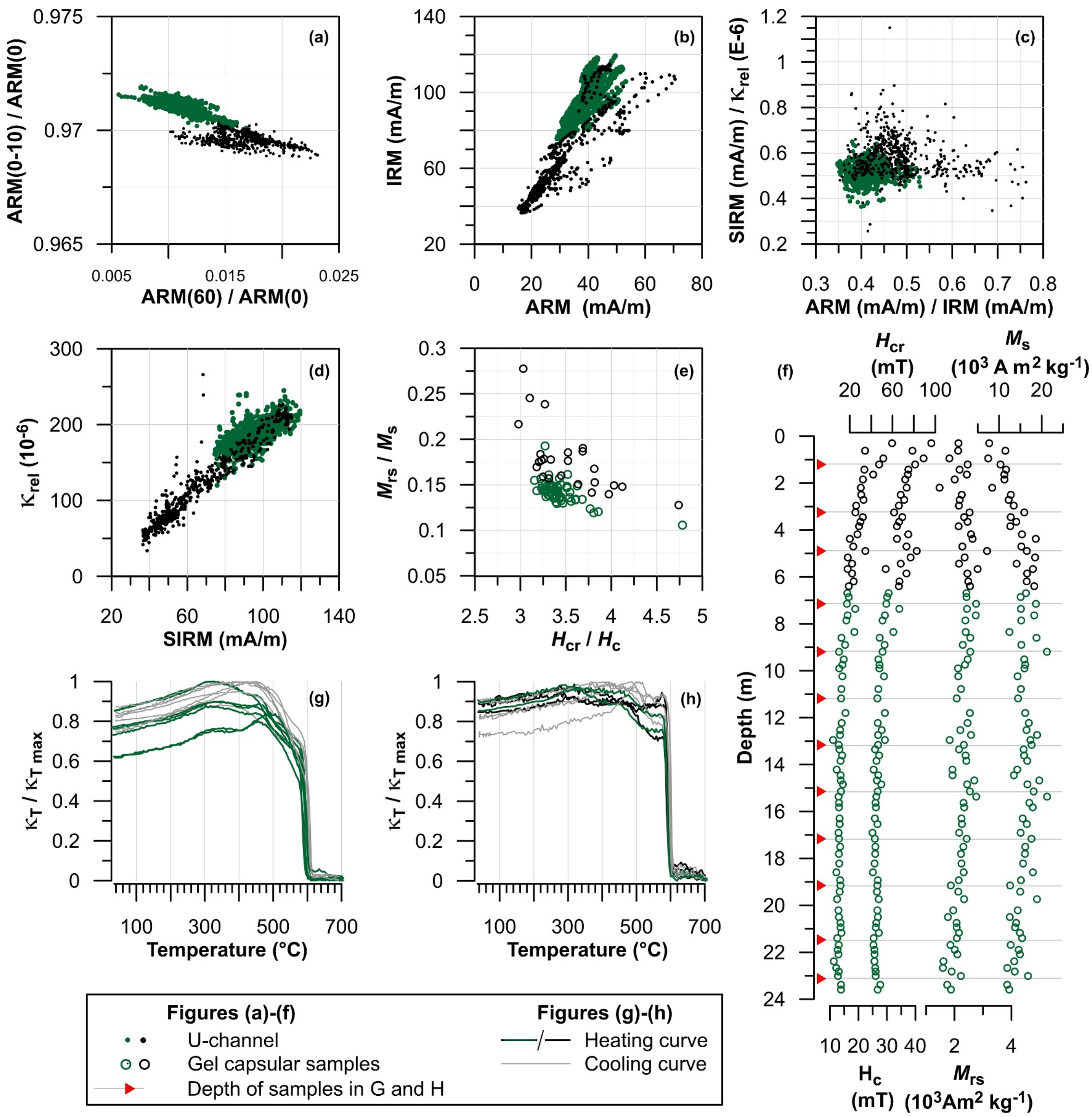

Figure 4. Diagrams showing measurements and related parameters for mineral magnetic characterization of core 506-48. The lower and upper unit are shown in green and black, respectively. (a–d): Bi-Plots of u-channel measurements. (e): Day plot. (f): downcore hysteresis parameters (from left to right) H_c, H_{cr}, M_{rs}, M_s. Red triangles in (f) indicate depth levels of samples used for κT-measurements of magnetically extracted minerals below 10 m depth (g) and above (h).

fraction with high coercivity does not exhibit a magnetization direction that differs from that of the ferrimagnetic minerals (see Section 4.2), it can be assumed that they consist of (partially) oxidized detrital minerals. Since the hysteresis loops show only a little gap between the branches, the influence of hematite and maybe goethite on the magnetic properties is probably small. Please note that although a decrease in concentration sensitive parameters accompanied by an increase in coercivity in the uppermost meters suggest magnetite dissolution that frequently is associated with sulfide formation, no magnetic sulfide minerals could be identified. However, as 15 years passed between the core recovery and the magnetic extraction, the sulfides may have already decomposed by the time of the measurements.

Overall, the mineral magnetic inventory appears to be composed of partially maghemized magnetite and titanomagnetite and a high coercivity phase which likely reflect detrital hematite. According to the mineral magnetic components and the domain states determined, the lake sediment probably carries post-detrital remanent magnetization (pDRM), which can reliably record and retain the primary acquired magnetization.

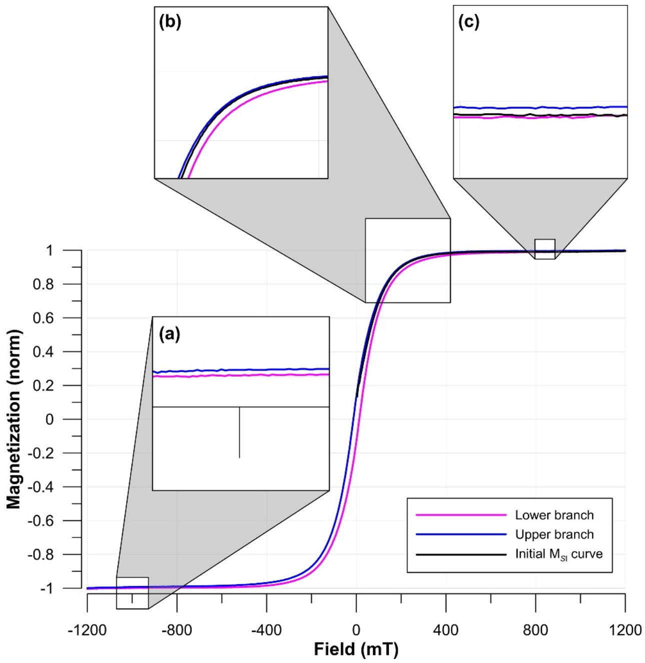

Figure 5. Hysteresis measurement of a sample from core section 9-02 (section depth: 79–80 cm) corresponding to a core depth and core age of 15.83–15.84 m and about 20.6 ka. Inset (a) The upper and lower branch of the hysteresis remaining slightly open in fields of 1 T. Inset (b) The ratio of the areas enclosed by the hysteresis branches and the M_{SI} curve. Inset (c) The gap between the upper and lower branches of the hysteresis loop, causing the ratio of E_t^{Δ}/E_{hys} to be indeterminate.

4.2. Paleosecular Variation, Relative Paleointensity, Virtual Geomagnetic Pole Positions

Due to the use of different AF steps in the PCA and stricter rejection criteria, the ChRM directions determined from all cores differ slightly from those Haflidason et al. (2022) determined from the same data set. This study, for example, omits the lowermost core section of core 506-51, the top and bottom parts of all core sections, and all measurements above 6.68 m (i.e., younger than 14.8 ka cal. BP) because of the presence of turbidites and core disturbances, not reached MDF_{NRM}, and measurement artifacts at core section ends. The accepted u-channel measurements unveil well-defined single-component magnetization (Figure 6) with 95% of the MAD values of the cores 506-48, 506-50 and 506-51 below 1.33°, 1.21°, and 1.83°, respectively. Frequently occurring viscous overprints were easily removed with AF fields of ≤15 mT. Although the residual remanence after AF demagnetization is relatively high, it is not assumed that the determined ChRM is biased, since the observed demagnetization paths in the Zijderveld diagrams migrate directly toward the origin (Figure 6).

The ChRM inclination values range between 55.7° and 89.4°N in all cores (Figure 7). The presented ChRM declination curves are the result of an iterative process in which the individual segments of all three cores were aligned relative to each other. The lowermost part (>21.9 ka) of the resultant ChRM declination curves shows major differences between the cores (Figure 7). Since the ChRM inclination is well correlated and quite steep, this misfit is assumed to be caused by an unfavorable signal-to-noise ratio of the horizontal component. In the period between 21.9 and 14.8 ka, the ChRM inclination and declination are characterized by a high degree of similarity between the three cores. Overall, this is a strong argument for the primary character of the magnetic signal, and the comparability of the recording efficiency as well as the degree of potential smoothing during pDRM acquisition in the two lakes.

The cores 506-48 and 506-50 largely meet the requirements for being good sedimentary RPI recorders as specified by Lisa Tauxe (1993) and Stoner and St-Onge (2007). The required homogeneity of the mineral magnetic assemblage and low variability in concentration and domain size are to a substantial extent provided (see Section 4.1). Only a few peaks in the RPI curves may be associated with fine layers with slightly differing grain size or composition (Figure 7). The minimal offset between RPI_{IRM} and RPI_{ARM} of core 506-48 indicates a slight change in coercivity along the core. Notwithstanding, the variations are small and most of the sediment

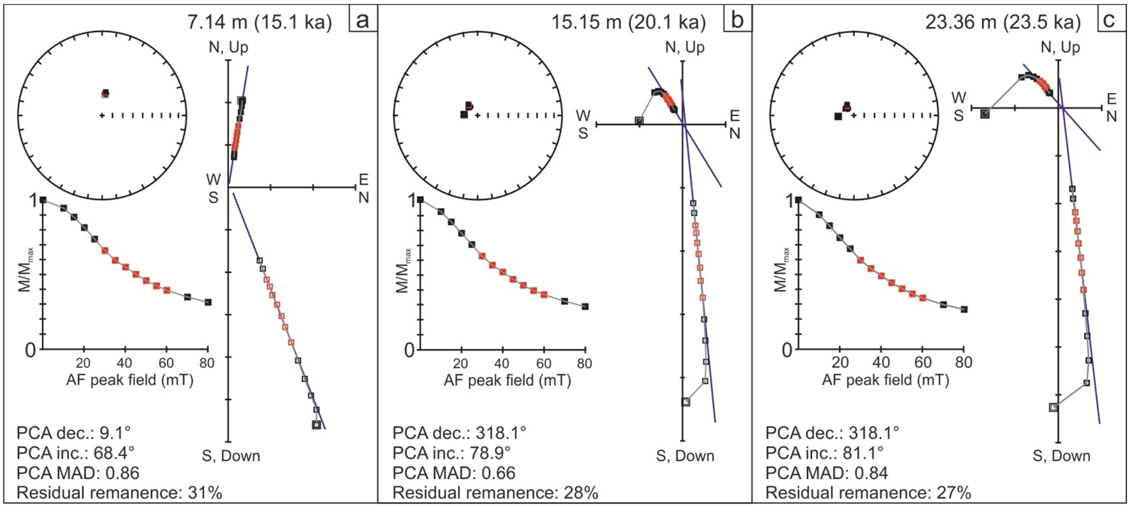

Figure 6. Representative demagnetization behavior from three depth levels in core 506-48 shown in equal area projections, Zijderveld plots (Zijderveld, 1967) with arbitrary units, and demagnetization-intensity biplots. Depth and corresponding age are shown. Measurement steps used for PCA are colored red. Open/closed squares indicate vertical/horizontal projections. The demagnetization paths of the samples from depths of 7.14 m (a), 15.15 m (b) and 23.36 m (c) migrate directly towards the origin.

sequence is homogenously composed. Thus, the very similar trends seen in the records from cores 506-48 and 506-50 are assumed to reflect variations in magnetic field intensity. The lowest RPI value is centered at around 20 ka cal. BP, coinciding with the anomalous directional behavior observed in the sediment sequence between 19.1 and 20.2 ka cal. BP, previously referred to as the Bolshoye Shchuchye event. The limits are set by the sudden changes in ChRM inclination in core 506-48. Singer et al. (2014) lists several incidences of geomagnetic excursions or anomalous magnetic field behavior in the period between 17 and 20 ka. In order to maintain clarity in the nomenclature, the term Hilina Pali geomagnetic excursion is mainly used for incidences happening in this period today (Table 1). In this update of the data first presented by Haflidason et al. (2022) we thus, will also refer only to Hilina Pali in the following.

Nevertheless, it still needs to be proven whether Hilina Pali in the sediment records presented in this study represent a directional anomaly or whether they meet the requirements for a geomagnetic excursion. Therefore, the VGP positions were determined for the period between 18.9 and 20.5 ka cal BP. For this, the cores from lakes Bol.S. and Mal.S. had to be azimuthally oriented. This was challenging, since the paleo directions obtained in the upper meters of the cores are not reliable, and predictions from spherical harmonic field models are heavily biased by scarce data coverage in the high latitudes (Panovska et al., 2019). Due to the striking similarity between the RPI records and the VGP paths of the Black Sea Stack and the Lake Bol.S. record (Figures 8 and 9), we tentatively assume that the records can be compared.

Therefore, we rotated the ChRM declination of the records from Lakes Bol.S. and Mal.S. in such a way that the VGP positions at the end of Hilina Pali lie close to those determined for the Black Sea Stack near Spitsbergen (Liu et al., 2020). The orientation of the declination and thus, of the VGP of the Black Sea cores, are based on Fisherian mean paleomagnetic directions and the α_{95} angle of confidence, determined from paired ChRM inclinations and declinations (Nowaczyk et al., 2012). The resulting VGP positions of the Lake Bol.S. and Lake Mal.S. records (Figure 8a) describe a clockwise loop that moves from the Arctic Ocean off Greenland and Canada, across the Greenland Sea to southern Greenland. From here, the VGP makes a northerly detour before following a path roughly parallel to the latitude to the Alaska-Canada border. After some residence time, the VGP moves across the Bering Sea to Svalbard. The largest distance of the VGP from the geographic North pole occurs in core 506-48 in the Bering Sea at 19.19 ka cal. BP. The VGP paths from all three cores show broadly the same course; none of them indicate that the VGP during this period has moved south of 50°N (Figure 8a). The small differences between the cores may be due to natural processes during remanence acquisition, the effects of core recovery, or small disturbances that may have been inflicted on the sediments during the u-channel sampling.

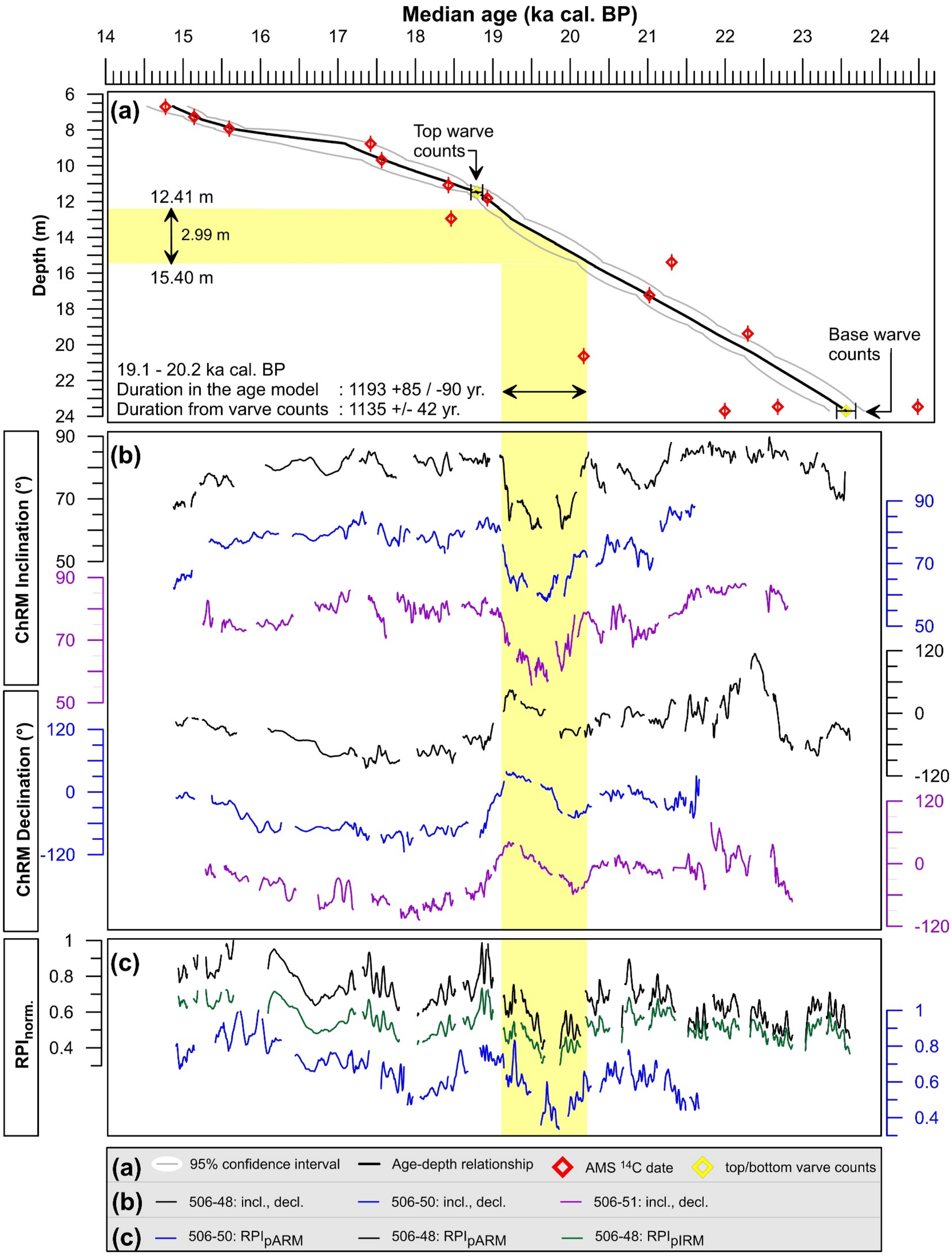

Figure 7. PSV and RPI variations with time. (a) Age model based on core 506-48 with 95% confidence interval (gray lines). (b) characteristic remanent magnetization (ChRM) inclination and ChRM declination of cores 506-48 (black), 506-50 (blue), and 506-51 (purple). (c) RPI of cores 506-48 (left axis: pARM: black, partial IRM green) and 506-50 (right axis: pARM: blue). The inclination deviation (Hilina Pali) is highlighted in yellow.

5. Discussion

The reproducibility of the paleomagnetic data from the two lake basins evidence that the hosted sediment successions provide exceptional high-resolution records of the geomagnetic field in northern Russia. However, only comparisons with other paleomagnetic records can show whether the directional anomaly discovered is an

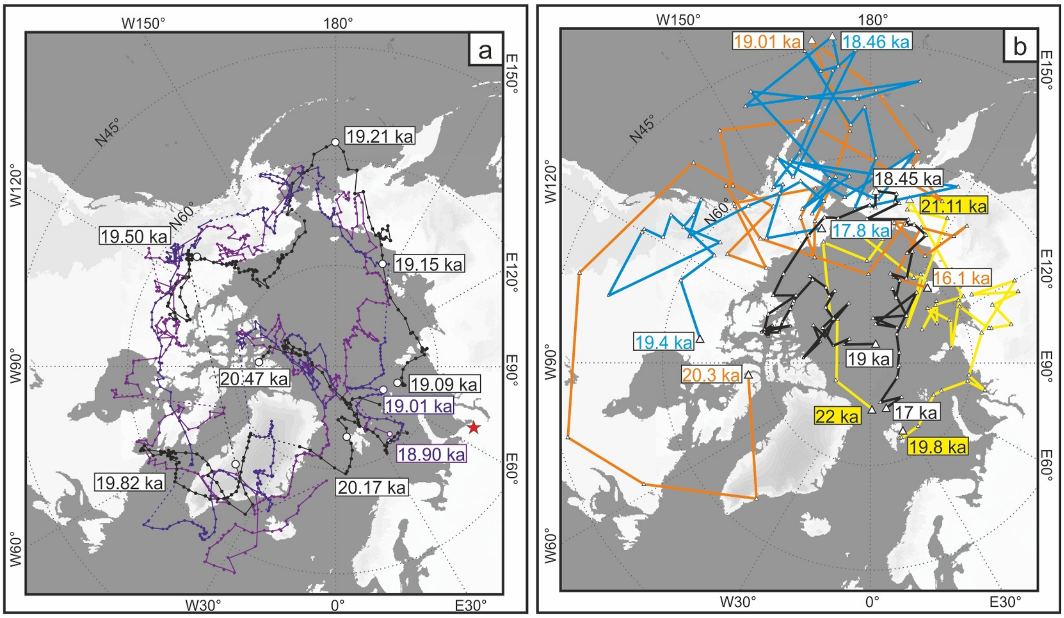

Figure 8. Virtual geomagnetic pole (VGP) paths of cores 506-48 (black), 506-50 (blue), and 506-51 (purple) between about 19 and 20.5 ka (a) and VGP paths of the Black Sea stack (black), core MRS_CS19 from the Sea of Marmara (blue), discrete samples from the Wilson Creek Beds, California (yellow) and Lake Baikal (orange) for comparison (b). Please note that the Lake Baikal stack was rotated clockwise by about 100° (see Section 4.3). The ages in the color-coded boxes refer to the larger open symbols on the map and indicate the age of the start and end points of the paths shown, as well as the age of the largest deviation to the south. The red star in a shows the location of lakes Bol.S. and Mal.S..

isolated regional feature of the Earth's magnetic field, or rather the regional expression of the globally described Hilina Pali geomagnetic excursion.

5.1. Comparisons With Magnetic Signals From Other Sediment Records

In theory, spatial and temporal uniformity of directional and intensity changes is needed, if a paleomagnetic feature should be used as a global marker. However, the reality is by far more complex (Landeau et al., 2022). Usually, the combination of non-dipolar and dipolar features of the geomagnetic field lead to very different geomagnetic field observations at different locations on Earth at the same time (Merrill & McFadden, 1994). Therefore, it is recommended to compare data sets only if they are no further than ∼2,000 km apart, as the consistency in fluctuations is most likely greater (Brown & Korte, 2016). This recommendation is difficult to follow for this study, as very few paleomagnetic records are available in northern Russia. For continental archives this is mainly due to glacial erosion, which has left only a few sediment sequences from the period before the Last Glacial Maximum (LGM) (Melles et al., 2022). For marine archives from the Arctic Ocean, low sedimentation rates (Levitan, 2015) and possible alteration processes (Wiers et al., 2019, 2020) limit the significance of paleomagnetic data (Valet et al., 2016). The few records within a 2,000 km circle around the lakes Bol.S. and Mal.S. (Figure 1), do not show weaker paleointensity or directional irregularities that can be confidently attributed to a geomagnetic anomaly.: While Lake Lama (Nowaczyk et al., 2012; Nowaczyk and Knies, 2000) reaches not far enough back in time, the shallowing of the paleomagnetic inclination in the cores GS191-01PC and GS191-02PC from the Barents Sea around 19.8 ka cal. BP (Caricchi et al., 2019, 2020, 2022) was attributed to a melt water pulse. However, insufficient resolution or hiatuses caused by the drilling position near the ice margin during the LGM could also be good reasons for not recording changes in field behavior in detail.

Besides, a deep lock-in depth may result in the absence of a paleomagnetic feature in a sedimentary archive, as might be the case in core Co1401 from Lake Levinson-Lessing (Scheidt et al., 2022). However, it should be noted that the absence of evidence at these locations does not necessarily prove that the paleomagnetic field anomaly found in cores 506-48, 506-50, and 506-51 is a local feature. In particular, the remarkable correlation of the RPI pattern of Bol.S. Lake with the field intensity fluctuations in the Black Sea Stack (Liu et al., 2020; about 3,350 km distant) and in the MRS_CS19 core from the Sea of Marmara (Makaroğlu et al., 2020; about 4,000 km distant)

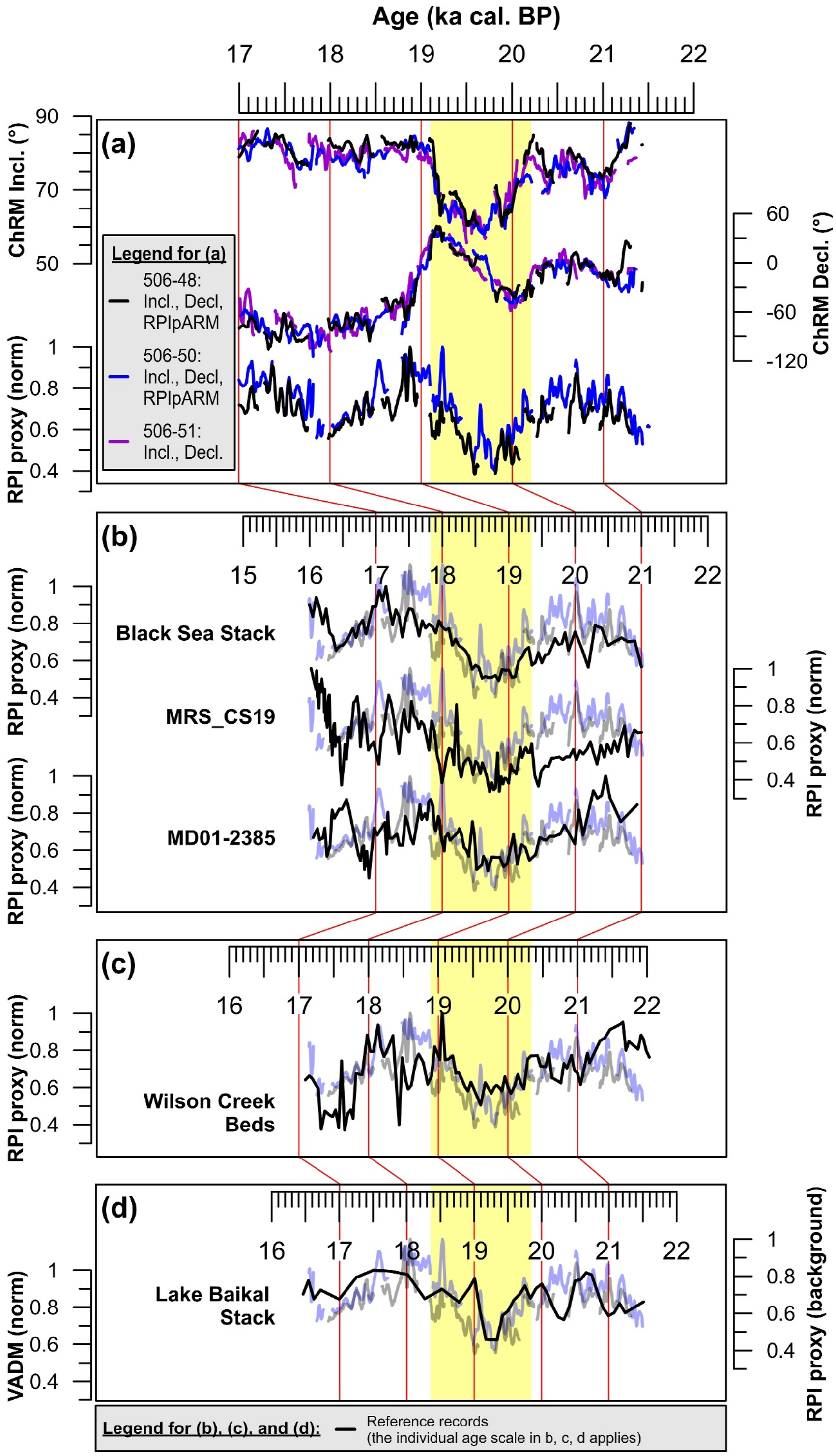

Figure 9. Paleomagnetic data from drill cores 506-48, 506-50, and 506-51 compared to RPI proxy data from selected reference records. Different age scales apply to the subsection (a-d). The age scales are linearly squeezed or extended and shifted to find the optimal match with the RPI data of Lake Bol.S.. The extent of the shift and change in extent is visualized with red lines. (a) characteristic remanent magnetization (ChRM) inclination, ChRM declination, and RPI_{pARM} of cores 506-48, 506-50, 506-51. The color code is provided in the inset legend. The recognized geomagnetic anomaly (Hilina Pali) is marked in yellow. For comparison, the RPI data from cores 506-48 and 506-50 and the yellow highlight are displayed in the background of all data sets shown in (b), (c), and (d). (b) RPI proxies of the Black Sea Stack (natural remanent magnetization (NRM)/anhysteretic remanent magnetization), Sea of Marmara core MRS_CS19 ($pNRM_{20–50mT}/pARM_{20–50mT}$), and core MD01-2385 from the eastern equatorial Pacific ($pNRM_{20–40mT}/pARM_{20–40mT}$). (c) RPI of the Wilson Creek Beds close to Mono Lake California (NRM/SIRM). (d) VADM of the long Lake Baikal Stack.

suggests that the distant archives recorded the same phenomenon (Figure 9). The fluctuations between the records shown are partly not larger than those between the parallel cores 506-48 and 506-50. The RPI recorded in core MD01-2385 from the continental margin northwest of Papua New Guinea (Dauchy-Tric et al., 2024; about 9,350 km distant), in the Wilson Creek Beds in the area of the Mono Lake in California (Lund et al., 2017; Lund et al., 1988; about 8,250 km distant), and in the Siberian Lake Baikal (Peck et al., 1996; 2,700 km distant) is also comparable, albeit somewhat less obvious (Figure 9). Unfortunately, the most recent study on a high-resolution sediment record from Lake Challa in equatorial East Africa documenting Hilina Pali (Di Chiara et al., 2025; 8,200 km distant) is lithologically too diverse to deduce the RPI. However, the available examples in Figure 9 already show that during the period when Hilina Pali is described, the paleomagnetic field reached a trough. Although caution is advised when comparing data sets from locations that are far apart, we do not consider the similarity of the RPI curves to be coincidental. The RPI suggests a globally recognizable decay of the dipole field, though the field remained clearly stronger than during the well documented Laschamps geomagnetic excursion, for example, (e.g., Liu et al., 2020).

The comparability of the globally distributed records includes also the VGPs determined from the sediment records in the Black Sea and the Sea of Marmara, whose maximum deviations are in the same area as those of lakes Bol.S. and Mal.S. during the time of the RPI minimum (Figure 8). Of course, one can argue that we used the location of the VGP position at the end of Hilina Pali determined from the Black Sea Stack for reorientation of the declination values of the presented records. However, the position would be similar if we had used the average VGP and the expected geocentric axial dipole for reorientation. In addition, it is not only the positions of the VGP tracks that are similar, but also the fundamental course that the VGPs are taking. In addition, also the VGP path of the Wilson Creek data set (Lund et al., 1988, 2017) is comparable (Figure 8b). It describes a clockwise loop like the one presented in Figure 8a and is comparable in shape to that of the Black Sea Stack. Yet, the Wilson Creek record is particularly interesting because its VGP path reconstructed is based on fully oriented discrete samples retrieved from outcrops. Thus, the ChRM declination values and the VGP path are not subject to the uncertainties associated with sediment cores that are not oriented with respect to the azimuth. By contrast, the declination of the sediment cores from the Sea of Marmara and Lake Baikal were reorientated using the expected geocentric axial dipole. In addition, the records contain a complete sequence with few or no gaps, allowing them to be aligned at the top to today's geomagnetic field. However, Peck et al. (1996) caution against considering their declination values valid until additional data confirm the record's orientation. We therefore rotated the declination determined at Lake Baikal by about 100° clockwise around the drilling site to bring the largest VGP deviation into line with the other data sets in the Bering Sea. However, no details can be discerned because the VGP path from Lake Baikal has a relatively low resolution and, like the data set from the Sea of Marmara, is very noisy. The VGP path determined from the sediment core MD01-2385 from the northwest margin of Papua-New Guinea and from the DeepChalla composite core from Lake Challa in East Africa are not depicted in Figure 8b, as their equatorial drilling locations result in an apparent fluctuation of the determined VGP positions between the hemispheres. However, the data on the sediment sequence of Lake Challa allows a comparison of its VGP latitudes with those of Lakes Bol.S. and Mal.S. (Figure 10). Although the resolution of the data from the DeepChalla composite core is much lower than that of the cores in this study, and the VGP latitudes between 20.5 ka and 21 ka show unnatural behavior, the similarity of the principal shape of the curves cannot be denied. One key difference, though, is that the VGP latitudes obtained from Lake Challa indicate a complete reversal, while those of the lake cores from northern Russia don't even show transitional directions. Contrary to the evidence presented by RPI and VGP above, this cannot be explained without the influence from non-dipole components of the Earth's magnetic field. Temporal oscillating flux patches causing inclination anomalies are frequently observed in paleomagnetic field models. Besides the high-latitudes, equatorial Africa appears to be affected in several model calculations (Amit et al., 2011; Constable et al., 2016; Panovska et al., 2019). The decay of the dipole field in combination with regional PSV patterns could lead to the VGP path found at Lake Challa. However, future model calculations must show which configuration of the geomagnetic field can best explain all observations presented.

5.2. Age and Duration of Hilina Pali

For our Russian lake cores the chronology of the geomagnetic feature labeled Hilina Pali can be delimited very precisely, because the age model is based on a floating varve chronology anchored by four radiocarbon dates on plant macro fossils (Figure 7; Table 1), which were found by the depositional model to be consistent with the varve count (Regnéll et al., 2019). Since VGPs do not deviate by at least 40–45° from the geographic pole, Hilina

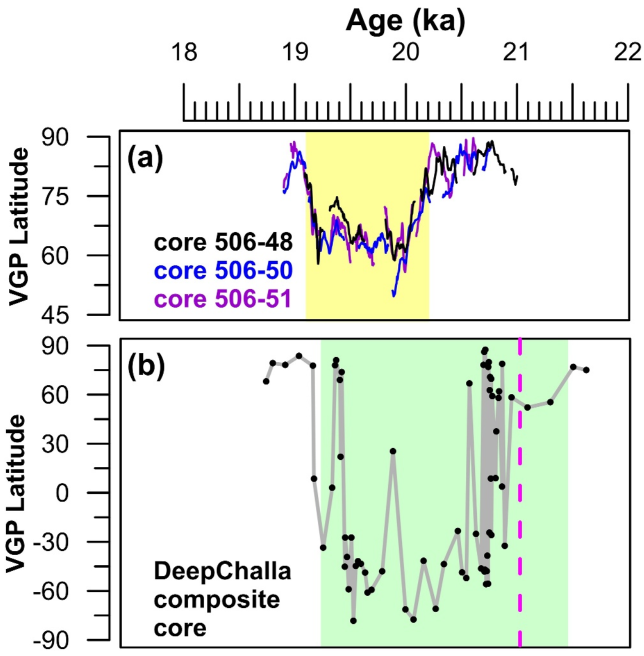

Figure 10. Comparison of virtual geomagnetic pole (VGP) latitudes during Hilina Pali. (a) The VGP latitudes determined from cores 506-48, 506-50 and 506-51. The yellow area illustrates the age range assigned to Hilina Pali based on the inclination deviation. (b) The VGP positions reported for the DeepChalla composite core using the age data of Baxter et al. (2023). The green area refers to the time interval that restricts Hilina Pali according to Di Chiara et al. (2025). However, a figure in the same study showing the VGP latitude versus depth indicates that Hilina Pali starts at the pink dashed line.

Pali cannot formally be categorized as a geomagnetic excursion in our records and the VGP ± 45° cut-off method cannot be applied to define the boundaries of the geomagnetic feature. For comparisons, we can instead use the inclination deviation between 19.1 and 20.2 ka in core 506-48 (Figures 7 and 9) or the deviation of the VGP latitude curve defining an interval between 19 ka and 20.3 ka (Figure 10). By counting varves, these intervals result in durations of 1,135 ± 35 years and 1,294 ± 44 years, respectively. The age and duration of Hilina Pali in our Russian lake sediment cores are compared to those from reference archives (Figures 9 and 10). All reference data sets are displayed using the age models established for the respective sediment sequences. The vertical extent of the yellow area on the individual age scales in Figure 9b–9d indicates the period during which the RPI pattern occurs in the reference records according to our correlation. The time intervals are defined for the Black Sea Stack, core MRS_CS19, and core MD01-2385 as 19.3 to 17.8 ka; a period of 20.3 to 18.9 ka is given for the Wilson Creek Beds, and at Lake Baikal the feature occurred between 19.8 and 18.4 ka.

An important question for the comparison of ages is whether geomagnetic features occur simultaneously worldwide. Different aspects must be considered when trying to answer this question. It is important to understand that the local paleomagnetic field is a linear transformation of the dipolar and non-dipolar components (Constable et al., 2016). Non-dipole features, such as flux patches, may have a strong influence on the local magnetic field vectors. This can cause VGP tracks and RPI patterns from two different positions to deviate widely from each other. However, if a superposition of a dominant axial dipole field is assumed, a decrease in the intensity of the Earth's magnetic field would occur at the same time in different locations. In this case, the age differences between the various Hilina Pali recordings may be related to the uncertainties inherent in any dating method. Additional uncertainties may arise from sample preservation, collection, and processing, measurement procedures, and the interpretation of dating results. Although we are convinced that the authors of all reference studies took great care in compiling their age models, we tentatively assume dating issues to cause most of the chronological variation in Figure 9. The age model of the Black Sea Stack, for example, which goes back up to 70 ka, is based on AMS^{14}C data that were refined by correlating ice-drifted debris and X-ray fluorescence protocols on the oxygen isotope data set (δ^{18}O) of the North Greenland Ice Core Project (NGRIP). In the period 17–21 ka, however, the NGRIP curve does not show any specific features. Hence the age model here is based primarily on two ^{14}C dates (Nowaczyk et al., 2012) for which a constant reservoir offset of 1,450 years is assumed (Kwiecien et al., 2008) while the marine calibration curve is characterized by considerable fluctuations (Reimer et al., 2020). Thus, small variations in age or variability in the reservoir effect would considerably affect the age of the geomagnetic feature associated with Hilina Pali. Similarly, the age model of the Wilson Creek data set has some degree of uncertainty, in the period of interest. The updated version of the Wilson Creek age model is related to the paleosecular variation (PSV) record from Pyramid Lake (Lund et al., 2017), which is based on ^{14}C dates, supplemented by GISP2-based age data for all correlatable PSV characteristics. Though, the age model appears to be robust, the ^{14}C dates are more than 25 years old and may suffer from some degree of contamination (Lund et al., 2017). Furthermore, a small mismatch in the PSV correlation can easily lead to the observed offset in age. Finally, Di Chiara et al. (2025) claim to have precisely delineate the age, duration, and extent of Hilina Pali at Lake Challa using the Baxter et al. (2023) age model of the sediment sequence of the composite core DeepChalla. Accordingly, Hilina Pali starts at 21.45 ka cal. BP (95% confidence interval: 21.04–21.74 ka cal. BP) in 19.29 m event-free sediment depth (mefd) and ends at 19.26 ka cal. BP (95% confidence interval: 18.87–19.63 ka cal. BP) in 17.21 mefd (Figure 10). Thus, the duration of the Hilina Pali geomagnetic excursion should be recorded in a 2.08 m thick layer and is constrained to about 2.2 ka. However, there is an issue with the age-depth relationship. Di Chiara et al. (2025) made available the VGP data only with depth and Baxter et al. (2023) provide dating results. According to Baxter et al. (2023) an age of 20.89 ka cal. BP (+0.18/–0.19) applies to a depth of 19.64 mefd. This is not consistent with the age of 21.45 ka cal. BP in 19.29 mefd stated by Di Chiara et al. (2025). In addition, the starting point of Hilina Pali shown by Di Chiara et al. (2025) in one figure of VGP latitudes versus depth corresponds to an age of about 21 ka cal. BP (pink dashed line in Figure 10) and is below a section with questionable VGP latitude data points that do not consistently indicate one hemisphere. However, the end of Hilina Pali at about 19 ka suits well with the age of VGP latitude deviation obtained from Lake Bol.S..

Apart from dating issues, a time lag between deposition and remanence acquisition can also affect the accuracy of the determined ages of paleomagnetic features. This lock-in effect may vary through a stratigraphic succession (Sagnotti et al., 2005) and can cause age offsets of up to several hundred years (Bliedtner et al., 2024). We assume a moderate to low lock-in depth for the sediments in Lake Bol.S., as the carbon content is low with values of 1%–2%, the sediment composition is largely uniform, and the sedimentation rates are quite high with mean values of 2.5 m/kyr (Regnéll et al., 2019). Although we are not able to quantify the age offset caused by the lock-in depth, due to the age constraints from varve counting, we are confident that the duration of the geomagnetic feature Hilina Pali is quite short with a duration of about 1,300 years. This may explain why it is not captured by sedimentary archives frequently.

6. Conclusion

A paleomagnetic directional anomaly found in well-dated sediment cores from the two lakes Bolshoye Shchuch'ye and Maloye Shchuch'ye, polar Ural Mountains, Arctic Russia, represents the proposed geomagnetic excursion Hilina Pali in unprecedented high resolution. According to AMS^{14}C dating and varve counting, it is characterized by relative low ChRM inclination and RPI values occurring in the period 20.2–19.1 ka cal. BP (1,135 ± 35 years). If the VGP latitude is used for constraining the geomagnetic feature, a slightly longer period between 19.0 and 20.3 ka cal. BP (1,294 ± 44 years) results. The VGP paths determined from directional data of all three sediment cores describe similar clockwise running loops with VGP positions always at latitudes higher than 55°N. Thus, according to the definition of Merrill and McFadden (1994), Hilina Pali in northern Russia cannot be classified as a true geomagnetic excursion, but maybe as an extreme secular variation feature. Greatest insights into the Earth magnetic field behavior during Hilina Pali are gained from the comparison with high-resolution sedimentary records from different regions of Earth. Although there are age offsets in the timing of Hilina Pali in the different records, which we tentatively assign to dating issues, the well correlating RPI and the similarity of the VGP path of most reference records suggest that the dipole field was dominant during Hilina Pali. However, a reference data set from Equatorial Africa shows (locally) reversed directions; here, the VGP positions shifted from the northern to the southern hemisphere and back again. Based on this study, we conclude that Hilina Pali is a globally occurring feature of the Earth's magnetic field characterized by a reduced dipole field. This can probably be used globally as a tool for correlation and dating of geoarchives if suitable material is available. Whether Hilina Pali is associated with transitional or even reversed directions may depend on the potential influence of non-dipole features of the Earth's magnetic field in the vicinity of the individual records. Future geomagnetic field model calculations must show how this observation can be explained.

Conflict of Interest

The authors declare no conflicts of interest relevant to this study.

Data Availability Statement

The data presented in the study is available at figshare data repository via Scheidt et al. (2025), with license CC-BY 4.0.

Acknowledgments
We acknowledge B. Reilly for his assistance in the Paleomagnetic and Environmental Magnetic Research Laboratory at the College of Earth, Ocean, and Atmospheric Sciences, Oregon State University. Thanks to A. Di Chiara, S.P. Lund, Ö. Makaroğlu and J.A. Peck for providing reference data. Core retrieval and u-channel measurements were funded by the Norwegian Research Council–Grant CHASE NRC 255415. S. Scheidt is funded by the Deutsche Forschungsgemeinschaft (DFG, German Research Foundation)–project number 521549505 under the Germany's Priority Program "Reconstructing the deep dynamics of planet Earth over geologic time (DeepDyn)" SPP2404-500707704. Open Access funding enabled and organized by Projekt DEAL.

References

Ahn, H.-S., Sohn, Y. K., Lee, J.-Y., & Kim, J. C. (2018). Preliminary paleomagnetic and rock magnetic results from 17 to 22 ka sediment of Jeju Island, Korea: Geomagnetic excursional behavior or rock magnetic anomalies? *Earth Planets and Space*, *70*(1), 78. https://doi.org/10.1186/s40623-018-0850-4

Amit, H., Korte, M., Aubert, J., Constable, C., & Hulot, G. (2011). The time-dependence of intense archeomagnetic flux patches. *Journal of Geophysical Research*, *116*(B12), B12106. https://doi.org/10.1029/2011JB008538

Banfield, J. F., Wasilewski, P. J., & Veblen, D. R. (1994). TEM study of relationships between the microstructures and magnetic properties of strongly magnetized magnetite and maghemite. *American Mineralogist*, *79*(7–8), 654–667.

Baxter, A. J., Verschuren, D., Peterse, F., Miralles, D. G., Martin-Jones, C. M., Maitituerdi, A., et al. (2023). Reversed Holocene temperature–moisture relationship in The Horn Of Africa. *Nature*, *620*(7973), 336–343. https://doi.org/10.1038/s41586-023-06272-5

Bjune, A. E., Alsos, G. I., Brendryen, J., Edwards, M. E., Haflidason, H., Johansen, M. S., et al. (2022). Rapid climate changes during the lateglacial and the early Holocene as seen from plant community dynamics in the polar Urals, Russia. *Journal of Quaternary Science*, *37*(5), 805–817. https://doi.org/10.1002/jqs.3352

Bliedtner, M., Haberzettl, T., Nowaczyk, N., Bazarradnaa, E., Zech, R., & Strobel, P. (2024). Assessing Lock-in depth and establishing a late Holocene paleomagnetic secular variation record from the Mongolian Altai. *Radiocarbon*, *66*(6), 1840–1851. https://doi.org/10.1017/RDC.2023.38

Brandt, U., Nowaczyk, N. R., Ramrath, A., Brauer, A., Mingram, J., Wulf, S., & Negendank, J. F. W. (1999). Palaeomagnetism of Holocene and Late Pleistocene sediments from Lago di Mezzano and Lago Grande di Monticchio (Italy): Initial results. *Quaternary Science Reviews*, *18*(7), 961–976. https://doi.org/10.1016/S0277-3791(99)00008-6

Brown, M. C., & Korte, M. (2016). A simple model for geomagnetic field excursions and inferences for palaeomagnetic observations. *Physics of the Earth and Planetary Interiors*, *254*, 1–11. https://doi.org/10.1016/j.pepi.2016.03.003

Caricchi, C., Campuzano, S. A., Sagnotti, L., Macrì, P., & Lucchi, R. G. (2022). Reconstruction of the virtual geomagnetic pole (VGP) path at high latitude for the last 22 kyr: The role of radial field flux patches as VGP attractor. *Earth and Planetary Science Letters*, *595*, 117762. https://doi.org/10.1016/j.epsl.2022.117762

Caricchi, C., Lucchi, R. G., Sagnotti, L., Macrì, P., Di Roberto, A., Del Carlo, P., et al. (2019). A high-resolution geomagnetic relative paleointensity record from the Arctic Ocean deep-water gateway deposits during the last 60 kyr. *Geochemistry, Geophysics, Geosystems*, *20*(5), 2355–2377. https://doi.org/10.1029/2018GC007955

Caricchi, C., Sagnotti, L., Campuzano, S. A., Lucchi, R. G., Macrì, P., Rebesco, M., & Camerlenghi, A. (2020). A refined age calibrated paleosecular variation and relative paleointensity stack for the NW Barents Sea: Implication for geomagnetic field behavior during the Holocene. *Quaternary Science Reviews*, *229*, 106133. https://doi.org/10.1016/j.quascirev.2019.106133

Channell, J. E. T., Singer, B. S., & Jicha, B. R. (2020). Timing of Quaternary geomagnetic reversals and excursions in volcanic and sedimentary archives. *Quaternary Science Reviews*, *228*, 106114. https://doi.org/10.1016/j.quascirev.2019.106114

Channell, J. E. T., Xuan, C., & Hodell, D. A. (2009). Stacking paleointensity and oxygen isotope data for the last 1.5 Myr (PISO-1500). *Earth and Planetary Science Letters*, *283*(1–4), 14–23. https://doi.org/10.1016/j.epsl.2009.03.012

Clark, H. C., & Kennett, J. P. (1973). Paleomagnetic excursion recorded in latest Pleistocene deep-sea sediments, Gulf of Mexico. *Earth and Planetary Science Letters*, *19*(2), 267–274. https://doi.org/10.1016/0012-821X(73)90127-1

Clarke, C. L., Alsos, I. G., Edwards, M. E., Paus, A., Gielly, L., Haflidason, H., et al. (2020). A 24,000-year ancient DNA and pollen record from the polar Urals reveals temporal dynamics of arctic and boreal plant communities. *Quaternary Science Reviews*, *247*, 106564. https://doi.org/10.1016/j.quascirev.2020.106564

Coe, R. S., Grommé, S., & Mankinen, E. A. (1978). Geomagnetic paleointensities from radiocarbon-dated lava flows on Hawaii and the question of the Pacific nondipole low. *Journal of Geophysical Research*, *83*(B4), 1740–1756. https://doi.org/10.1029/JB083iB04p01740

Constable, C., Korte, M., & Panovska, S. (2016). Persistent high paleosecular variation activity in southern hemisphere for at least 10 000 years. *Earth and Planetary Science Letters*, *453*, 78–86. https://doi.org/10.1016/j.epsl.2016.08.015

Dauchy-Tric, L., Carlut, J., Bassinot, F., & Valet, J.-P. (2024). High-resolution relative paleointensities over the last 40 ka from marine sediments in the western equatorial Pacific: Magnetic events and interhemispheric correlation. *Quaternary Science Reviews*, *337*, 108800. https://doi.org/10.1016/j.quascirev.2024.108800

Day, R., Fuller, M., & Schmidt, V. A. (1977). Hysteresis properties of titanomagnetites; grain-size and compositional dependence. *Physics of the Earth and Planetary Interiors*, *13*(4), 260–267. https://doi.org/10.1016/0031-9201(77)90108-X

Di Chiara, A., Karloukovski, V., Maher, B. A., Van Daele, M., Van der Meeren, T., & Verschuren, D. (2025). A continuous 150-kyr record of geomagnetic field variations from Lake chala, eastern equatorial Africa. *Geochemistry, Geophysics, Geosystems*, *26*(4), e2024GC011933. https://doi.org/10.1029/2024GC011933

Dushin, V. A., Serdyukova, O. P., Malyugin, A. A., Nikulina, I. A., Kozmin, V. S., Burmako, P. L., et al. (2009). *State geological Map of the Russian Federation 1:200 000. Polar ural series. Sheet Q-42-I, II (laborovaya)*. VSEGEI.

Earth google. (2025). Landsat/copernicus, airbus, maxar technologies, CNES/airbus, pictures taken: 1.1.2021–5.8.2024 (some pictures without date), camera 86 km, 67°51'25'N to 66°22'55'E, 272 m. Retrieved from https://earth.google.com.Satellitemapwithdatafrom

Eldegard, R. F. (2019). Glasiasjons-og klimahistorie de siste 22 000 år, basert på sedimentstratigrafi i Maloya Shchuchye, Polar Ural, Russland. MSc thesis. *The University of Bergen*.

Fabian, K. (2003). Some additional parameters to estimate domain state from isothermal magnetization measurements. *Earth and Planetary Science Letters*, *213*(3–4), 337–345. https://doi.org/10.1016/S0012-821X(03)00329-7

Fabian, K. (2006). Approach to saturation analysis of hysteresis measurements in rock magnetism and evidence for stress dominated magnetic anisotropy in young mid-ocean ridge basalt. *Physics of the Earth and Planetary Interiors*, *154*(3–4), 299–307. https://doi.org/10.1016/j.pepi.2005.06.016

Fabian, K., & von Dobeneck, T. (1997). Isothermal magnetization of samples with stable preisach function: A survey of hysteresis, remanence, and rock magnetic parameters. *Journal of Geophysical Research*, *102*(B8), 17659–17677. https://doi.org/10.1029/97JB01051

Gehring, A. U., Fischer, H., Louvel, M., Kunze, K., & Weidler, P. G. (2009). High temperature stability of natural maghemite: A magnetic and spectroscopic study. *Geophysical Journal International*, *179*(3), 1361–1371. https://doi.org/10.1111/j.1365-246X.2009.04348.x

Haflidason, H., Brendryen, J., Eldegard, R. F., Mangerud, J., Ólafsdóttir, S., Regnéll, C., & Svendsen, J. I. (2022). High-resolution chronology of 24 000-year long cores from two Lakes in the polar Urals, Russia, correlated with palaeomagnetic inclination records with a distinct event about 20 000 years ago. *Journal of Quaternary Science*, *37*(5), 778–789. https://doi.org/10.1002/jqs.3391

Haflidason, H., Regnéll, C., Pyne-O'Donnell, S., & Svendsen, J. I. (2019a). Extending the known distribution of the vedde ash into Siberia: Occurrence in Lake sediments from the timan ridge and the Ural Mountains, northern Russia. *Boreas*, *48*(2), 444–451. https://doi.org/10.1111/bor.12354

Haflidason, H., Zweidorff, J. L., Baumer, M., Gyllencreutz, R., Svendsen, J. I., Gladysh, V., & Logvina, E. (2019b). The lastglacial and Holocene seismostratigraphy and sediment distribution of Lake bolshoye Shchuchye, polar Ural Mountains, arctic Russia. *Boreas*, *48*(2), 452–469. https://doi.org/10.1111/bor.12387

Kirschvink, J. L. (1980). The least-squares line and plane and the analysis of palaeomagnetic data. *Geophysical Journal of the Royal Astronomical Society*, *62*(3), 699–718. https://doi.org/10.1111/j.1365-246x.1980.tb02601.x

Kotov, S., & Paelike, H. (2018). QAnalySeries–A cross-platform time series tuning and analysis tool. In *Paper presented at the American geophysical union, fall meeting 2018*. Retrieved from https://ui.adsabs.harvard.edu/abs/2018AGUFMPP53D1230K

Kwiecien, O., Arz, H. W., Lamy, F., Wulf, S., Bahr, A., Röhl, U., & Haug, G. H. (2008). Estimated reservoir ages of the black sea since the last glacial. *Radiocarbon*, *50*(1), 99–118. https://doi.org/10.1017/S0033822200043393

Laj, C., & Channell, J. E. T. (2007). 5.10 - Geomagnetic excursions. In G. Schubert (Ed.), *Treatise on geophysics* (pp. 373–416). Elsevier.

Laj, C., Guillou, H., & Kissel, C. (2014). Dynamics of the earth magnetic field in the 10–75 kyr period comprising the Laschamp and Mono Lake excursions: New results from the French Chaîne des Puys in a global perspective. *Earth and Planetary Science Letters*, *387*, 184–197. https://doi.org/10.1016/j.epsl.2013.11.031

Laj, C., Kissel, C., Scao, V., Beer, J., Thomas, D. M., Guillou, H., et al. (2002). Geomagnetic intensity and inclination variations at Hawaii for the past 98 kyr from core SOH-4 (Big island): A new study and a comparison with existing contemporary data. *Physics of the Earth and Planetary Interiors*, *129*(3), 205–243. https://doi.org/10.1016/S0031-9201(01)00291-6

Landeau, M., Fournier, A., Nataf, H.-C., Cébron, D., & Schaeffer, N. (2022). Sustaining Earth's magnetic dynamo. *Nature Reviews Earth & Environment*, *3*(4), 255–269. https://doi.org/10.1038/s43017-022-00264-1

Lenz, M. M., Andreev, A., Nazarova, L., Syrykh, L. S., Scheidt, S., Haflidason, H., et al. (2022). Climate, glacial and vegetation history of the polar ural Mountains since c. 27 cal ka bp, inferred from a 54 m long sediment core from Lake bolshoye shchuchye. *Journal of Quaternary Science*, *37*(5), 17–835. https://doi.org/10.1002/jqs.3400

Leonard, G. S., Calvert, A. T., Hopkins, J. L., Wilson, C. J. N., Smid, E. R., Lindsay, J. M., & Champion, D. E. (2017). High-precision 40Ar/39Ar dating of Quaternary basalts from Auckland Volcanic field, New Zealand, with implications for eruption rates and paleomagnetic correlations. *Journal of Volcanology and Geothermal Research*, *343*, 60–74. https://doi.org/10.1016/j.jvolgeores.2017.05.033

Levitan, M. A. (2015). Sedimentation rates in the Arctic Ocean during the last five marine isotope stages. *Oceanology*, *55*(3), 425–433. https://doi.org/10.1134/S000143701503011X

Lisé-Pronovost, A., St-Onge, G., Gogorza, C., Haberzettl, T., Preda, M., Kliem, P., et al. (2013). High-resolution paleomagnetic secular variations and relative paleointensity since the Late Pleistocene in southern South America. *Quaternary Science Reviews*, *71*, 91–108. https://doi.org/10.1016/j.quascirev.2012.05.012

Liu, J., Nowaczyk, N. R., Frank, U., & Arz, H. W. (2018). A 20–15 ka high-resolution paleomagnetic secular variation record from Black Sea sediments – No evidence for the "hilina Pali excursion"? *Earth and Planetary Science Letters*, *492*, 174–185. https://doi.org/10.1016/j.epsl.2018.04.014

Liu, J., Nowaczyk, N. R., Panovska, S., Korte, M., & Arz, H. W. (2020). The Norwegian-Greenland sea, the Laschamps, and the Mono Lake Excursions recorded in a black sea sedimentary sequence spanning from 68.9 to 14.5 ka. *Journal of Geophysical Research: Solid Earth*, *125*(8), e2019JB019225. https://doi.org/10.1029/2019JB019225

Lohne, Ø. S., Mangerud, J., & Birks, H. H. (2013). Precise 14C ages of the vedde and saksunarvatn ashes and the younger dryas boundaries from Western Norway and their comparison with the Greenland ice core (GICC05) chronology. *Journal of Quaternary Science*, *28*(5), 490–500. https://doi.org/10.1002/jqs.2640

Lund, S. P., Benson, L., Negrini, R., Liddicoat, J., & Mensing, S. (2017). A full-vector paleomagnetic secular variation record (PSV) from pyramid Lake (nevada) from 47–17 ka: Evidence for the successive Mono Lake and laschamp excursions. *Earth and Planetary Science Letters*, *458*, 120–129. https://doi.org/10.1016/j.epsl.2016.09.036

Lund, S. P., Liddicoat, J. C., Lajoie, K. R., Henyey, T. L., & Robinson, S. W. (1988). Paleomagnetic evidence for long-term (104 year) memory and periodic behavior in the earth's core dynamo process. *Geophysical Research Letters*, *15*(10), 1101–1104. https://doi.org/10.1029/GL015i010p01101

Lurcock, P. C., & Wilson, G. S. (2012). PuffinPlot: A versatile, user-friendly program for paleomagnetic analysis. *Geochemistry, Geophysics, Geosystems*, *13*(6), Q06Z45. https://doi.org/10.1029/2012GC004098

Makaroğlu, Ö., Nowaczyk, N. R., Eriş, K. K., & Çağatay, M. N. (2020). High-resolution palaeomagnetic record from Sea of Marmara sediments for the last 70 ka. *Geophysical Journal International*, *222*(3), 2024–2039. https://doi.org/10.1093/gji/ggaa281

Melles, M., Svendsen, J. I., Fedorov, G., Brigham-Grette, J., & Wagner, B. (2022). Quaternary environmental and climatic history of the northern high latitudes–Recent contributions and perspectives from Lake sediment records. *Journal of Quaternary Science*, *37*(5), 721–728. https://doi.org/10.1002/jqs.3456

Merrill, R. T., & McFadden, P. L. (1994). Geomagnetic field stability: Reversal events and excursions. *Earth and Planetary Science Letters*, *121*(1), 57–69. https://doi.org/10.1016/0012-821X(94)90031-0

Muxworthy, A. R., Turney, J. N., Qi, L., Baker, E. B., Perkins, J. R., & Abdulkarim, M. A. (2023). Interpreting high-temperature magnetic susceptibility data of natural systems. *Frontiers in Earth Science*, *11*, 1171200. https://doi.org/10.3389/feart.2023.1171200

Nawrocki, J., Bogucki, A., Łanczont, M., Werner, T., Standzikowski, K., & Pańczyk, M. (2018). The hilina pali palaeomagnetic excursion and possible self-reversal in the loess from Western Ukraine. *Boreas*, *47*(3), 954–966. https://doi.org/10.1111/bor.12305

Nowaczyk, N., Antonow, M., Knies, J., & Spielhagen, R. F. (2003). Further rock magnetic and chronostratigraphic results on reversal excursions during the last 50 ka as derived from northern high latitudes and discrepancies in precise AMS 14C dating. *Geophysical Journal International*, *155*(3), 1065–1080. https://doi.org/10.1111/j.1365-246X.2003.02115.x

Nowaczyk, N., Arz, H. W., Frank, U., Kind, J., & Plessen, B. (2012). Dynamics of the laschamp geomagnetic excursion from black Sea sediments. *Earth and Planetary Science Letters*, *351–352*, 54–69. https://doi.org/10.1016/j.epsl.2012.06.050

Nowaczyk, N., & Knies, J. (2000). Magnetostratigraphic results from the eastern Arctic Ocean: AMS ^{14}C ages and relative palaeointensity data of the Mono Lake and Laschamp geomagnetic reversal excursions. *Geophysical Journal International*, *140*(1), 185–197. https://doi.org/10.1046/j.1365-246x.2000.00001.x

Oda, H., & Xuan, C. (2014). Deconvolution of continuous paleomagnetic data from pass-through magnetometer: A new algorithm to restore geomagnetic and environmental information based on realistic optimization. *Geochemistry, Geophysics, Geosystems*, *15*(10), 3907–3924. https://doi.org/10.1002/2014GC005513

Oda, H., Xuan, C., & Yamamoto, Y. (2016). Toward robust deconvolution of pass-through paleomagnetic measurements: New tool to estimate magnetometer sensor response and laser interferometry of sample positioning accuracy. *Earth Planets and Space*, *68*(1), 109. https://doi.org/10.1186/s40623-016-0493-2

Özdemir, Ö. (1987). Inversion of titanomaghemites. *Physics of the Earth and Planetary Interiors*, *46*(1), 184–196. https://doi.org/10.1016/0031-9201(87)90181-6

Panovska, S., Korte, M., & Constable, C. G. (2019). One hundred thousand years of geomagnetic field evolution. *Reviews of Geophysics*, *57*(4), 1289–1337. https://doi.org/10.1029/2019RG000656

Peck, J. A., King, J. W., Colman, S. M., & Kravchinsky, V. A. (1996). An 84-kyr paleomagnetic record from the sediments of Lake Baikal, Siberia. *Journal of Geophysical Research*, *101*(B5), 11365–11385. https://doi.org/10.1029/96JB00328

Petrovský, E., & Kapička, A. (2006). On determination of the curie point from thermomagnetic curves. *Journal of Geophysical Research*, *111*(B12), B12S27. https://doi.org/10.1029/2006jb004507

Ramsey, C. B. (2008). Deposition models for chronological records. *Quaternary Science Reviews*, *27*(1), 42–60. https://doi.org/10.1016/j.quascirev.2007.01.019

Ramsey, C. B. (2009a). Bayesian analysis of radiocarbon dates. *Radiocarbon*, *51*(1), 337–360. https://doi.org/10.1017/S0033822200033865

Ramsey, C. B. (2009b). Dealing with outliers and offsets in radiocarbon dating. *Radiocarbon*, *51*(3), 1023–1045. https://doi.org/10.1017/s0033822200034093

Ramsey, C. B., & Lee, S. (2013). Recent and planned developments of the program OxCal. *Radiocarbon*, *55*(2), 720–730. https://doi.org/10.1017/S0033822200057878

Regnéll, C., Haflidason, H., Mangerud, J., & Svendsen, J. I. (2019). Glacial and climate history of the last 24 000 years in the polar ural Mountains, Arctic Russia, inferred from partly varved lake sediments. *Boreas*, *48*(2), 432–443. https://doi.org/10.1111/bor.12369

Reimer, P. J., Austin, W. E. N., Bard, E., Bayliss, A., Blackwell, P. G., Bronk Ramsey, C., et al. (2020). The IntCal20 northern hemisphere radiocarbon age calibration curve (0–55 CAL kBP). *Radiocarbon*, *62*(4), 1–33. https://doi.org/10.1017/RDC.2020.41

Roberts, A. P., Hu, P., Harrison, R. J., Heslop, D., Muxworthy, A. R., Oda, H., et al. (2019). Domain state diagnosis in rock magnetism: Evaluation of potential alternatives to the Day diagram. *Journal of Geophysical Research: Solid Earth*, *124*(6), 5286–5314. https://doi.org/10.1029/2018JB017049

Sagnotti, L., Budillon, F., Dinarès-Turell, J., Iorio, M., & Macrì, P. (2005). Evidence for a variable paleomagnetic lock-in depth in the Holocene sequence from the Salerno Gulf (Italy): Implications for "high-resolution" paleomagnetic dating. *Geochemistry, Geophysics, Geosystems*, *6*(11), Q11013. https://doi.org/10.1029/2005GC001043

Scheidt, S., Egli, R., Frederichs, T., Hambach, U., & Rolf, C. (2017). A mineral magnetic characterization of the Plio-Pleistocene fluvial infill of the Heidelberg Basin (Germany). *Geophysical Journal International*, *210*(2), 743–764. https://doi.org/10.1093/gji/ggx154

Scheidt, S., Lenz, M., Egli, R., Brill, D., Klug, M., Fabian, K., et al. (2022). A 62 kyr geomagnetic palaeointensity record from the Taymyr Peninsula, Russian Arctic. *Geochronology*, *4*(1), 87–107. https://doi.org/10.5194/gchron-4-87-2022

Scheidt, S., Olafsdottir, S., Brendryen, J., Nowaczyk, N. R., Svendsen, J. I., & Haflidason, H. (2025). Palaeomagnetic and mineral magnetic analyses of sediment cores from the lakes bolshoye Shchuch'ye and maloye Shchuch'ye in the polar Ural Mountains, Russia [dataset]. *figshare*. https://doi.org/10.6084/m9.figshare.c.7784627

Singer, B. S., Guillou, H., Jicha, B. R., Zanella, E., & Camps, P. (2014). Refining the Quaternary geomagnetic instability time scale (GITS): Lava flow recordings of the Blake and post-blake excursions. *Quaternary Geochronology*, *21*, 16–28. https://doi.org/10.1016/j.quageo.2012.12.005

Stoner, J. S., & St-Onge, G. (2007). Chapter three magnetic stratigraphy in paleoceanography: Reversals, excursions, paleointensity, and secular variation. In *Proxies in late Cenozoic paleoceanography* (pp. 99–138).

Svendsen, J. I., Færseth, L. M. B., Gyllencreutz, R., Haflidason, H., Henriksen, M., Hovland, M. N., et al. (2019). Glacial and environmental changes over the last 60 000 years in the Polar ural Mountains, arctic Russia, inferred from a high-resolution Lake record and other observations from adjacent areas. *Boreas*, *48*(2), 407–431. https://doi.org/10.1111/bor.12356

Tauxe, L. (1993). Sedimentary records of relative paleointensity of the geomagnetic field: Theory and practice. *Reviews of Geophysics*, *31*(3), 319–354. https://doi.org/10.1029/93RG01771

Tauxe, L., Pick, T., & Kok, Y. S. (1995). Relative paleointensity in sediments: A pseudo-thellier approach. *Geophysical Research Letters*, *22*(21), 2885–2888. https://doi.org/10.1029/95GL03166

Teanby, N., Laj, C., Gubbins, D., & Pringle, M. (2002). A detailed palaeointensity and inclination record from drill core SOH1 on Hawaii. *Physics of the Earth and Planetary Interiors*, *131*(2), 101–140. https://doi.org/10.1016/S0031-9201(02)00032-8

Valet, J.-P., Meynadier, L., Simon, Q., & Thouveny, N. (2016). When and why sediments fail to record the geomagnetic field during polarity reversals. *Earth and Planetary Science Letters*, *453*, 96–107. https://doi.org/10.1016/j.epsl.2016.07.055

Verosub, K. L., & Banerjee, S. K. (1977). Geomagnetic excursions and their paleomagnetic record. *Reviews of Geophysics*, *15*(2), 145–155. https://doi.org/10.1029/RG015i002p00145

Wiers, S., Snowball, I., O'Regan, M., & Almqvist, B. (2019). Late Pleistocene chronology of sediments from the yermak Plateau and uncertainty in dating based on geomagnetic excursions. *Geochemistry, Geophysics, Geosystems*, *20*(7), 3289–3310. https://doi.org/10.1029/2018GC007920

Wiers, S., Snowball, I., O'Regan, M., Pearce, C., & Almqvist, B. (2020). The Arctic Ocean manganese cycle, an overlooked mechanism in the anomalous palaeomagnetic sedimentary record. *Frontiers in Earth Science*, *8*(75), 75. https://doi.org/10.3389/feart.2020.00075

Williams, W., Moreno, R., Muxworthy, A. R., Paterson, G. A., Nagy, L., Tauxe, L., et al. (2024). Vortex magnetic domain state behavior in the day plot. *Geochemistry, Geophysics, Geosystems*, *25*(8), e2024GC011462. https://doi.org/10.1029/2024GC011462

Xu, X., Qiang, X., Yang, Z., Zhao, H., Fu, C., & Wang, Q. (2024). Magnetostratigraphy and relative paleointensity study of a late Quaternary lacustrine sediment sequence from southwest China and its chronological significance. *Palaeogeography, Palaeoclimatology, Palaeoecology*, *640*, 112067. https://doi.org/10.1016/j.palaeo.2024.112067

Xuan, C., & Channell, J. E. T. (2009). UPmag: MATLAB software for viewing and processing u channel or other pass-through paleomagnetic data. *Geochemistry, Geophysics, Geosystems*, *10*(10), Q10Y07. https://doi.org/10.1029/2009GC002584

Zijderveld, J. (1967). AC demagnetization of rocks: Analysis of results. In D. Collinson, K. Creer, & S. Runcorn (Eds.), *Methods in paleomagnetism* (Vol. 1, pp. 254–286). https://doi.org/10.1016/b978-1-4832-2894-5.50049-5